Transcriptomics and proteomics revealed sex differences in human pulmonary microvascular endothelial cells

Daria S. Kostyunina[1,2], Nikolai V. Pakhomov[1,2], Amina Jouida[1,2], Eugene Dillon[2], John A. Baugh[1,2], Paul McLoughlin[1,2]

1. School of Medicine, University College Dublin, Dublin, Ireland

2. Conway Institute, University College Dublin, Dublin, Ireland

Running title (60 characters)

Sex differences in pulmonary microvascular endothelial cells

Abstract (250 words)

Marked sexual dimorphism is displayed in the onset and progression of pulmonary hypertension (PH). Females more commonly develop pulmonary arterial hypertension (PAH), yet females with PAH and other types of PH have better survival than males. Pulmonary microvascular endothelial cells play a crucial role in the pulmonary vascular remodelling and increased pulmonary vascular resistance in PH. Given this background, we hypothesized that there are sex differences in the pulmonary microvascular endothelium basally and in response to hypoxia that are independent of the sex hormone environment. Human pulmonary microvascular endothelial cells (HPMECs) from healthy male and female donors, cultured under physiological shear stress, were analysed using RNA sequencing and label-free quantitative proteomics. Gene set enrichment analysis identified a number of sex different pathways both in normoxia and hypoxia, including pathways that regulate cell proliferation. *In vitro*, rate of proliferation in female HPMECs was lower than in male HPMECs, a finding that supports the omics results. Interestingly, thrombospondin1, an inhibitor of proliferation, was more highly expressed in female than in male cells. These results demonstrate for the first time important differences between female and male HPMECs that persist in the absence of sex hormone differences and identify novel pathways for further investigation that may contribute to sexual dimorphism in pulmonary hypertensive diseases.

Introduction

Males and females display sex dimorphism across all tissues in the body in the healthy state and in many diseases (1, 2). Sex differences in gene expression are detected in the embryo as early as the eight cell stage, before the development of gonads (3). In the adult sex differences are present not only in the reproductive system but also in other systems, including the immune, nervous and cardiovascular systems (2, 4, 5). Biological differences between male and female organisms arise either due to sex hormone effects or due to sex chromosome effects (6).

Pulmonary hypertension (PH) is a disease in which marked sexual dimorphism is observed. PH is characterised by remodelling and vasoconstriction of pulmonary arterioles, which causes a progressive rise in pulmonary vascular resistance (PVR) (7). This results in an

increased load on the right ventricle, which causes right ventricular hypertrophy and in the more severe forms of the disease, such as pulmonary arterial hypertension (PAH), leads to right heart failure and premature death (7). The most common and severe forms of PH develop in the third decade or later in life (7). Females develop pulmonary arterial hypertension (PAH) 1.5-4.0 times more commonly than males (8–10). However, females with PAH and other types of PH have better survival than males (11–13). Most of the studies of sex differences in PH have focused on the role of the sex hormones (14). For example, estrogens have been shown to have cardioprotective effects on right ventricular function, which might explain why females with PH have a better outcome than males but cannot fully account for the higher incidence of the disease in females (15, 16).

Pulmonary microvascular endothelial cells play a crucial role in pulmonary vascular remodelling in PH and display different responses when compared to endothelial cells from other regions and conduit arteries, such as pulmonary artery (17, 18). Sex differences have been detected in cells from different organs, isolated from males and females and cultured in the absence of sex hormones (19–32). In pulmonary vascular cells, sex differences have been detected in human pulmonary artery endothelial cells (HPAECs), mouse lung endothelial cells (MLECs) and foetal HPMECs (19, 25, 33). However, sex differences in adult human pulmonary microvascular endothelial cells have not been studied.

More recently, it has been shown that sex hormone-independent mechanisms, i.e. the sex chromosomes, also contribute to the sex differences in PH (34–36). For example, in hypoxia induced pulmonary hypertension in mice, the presence of a Y chromosome attenuated the development of the disease (34, 35). This protective effect was largely due to the Y-encoded gene Uty (Ubiquitously Transcribed Tetratricopeptide Repeat Containing, Y-Linked), which reduced the pro-inflammatory cytokines and protected against pulmonary artery endothelial cell apoptosis (35). Another Y-encoded gene, the transcription factor SRY (Sex Determining Region Y), might play a role in sex differences in PH as it induces increased expression of BMPR2 (37). Reduction of BMPR2-mediated signalling, either due to loss-of-function mutations or antagonists of ligand binding, plays an important role in the development of multiple forms of PH and the presence of SRY in males may protect against the loss of BMPR2 signalling (38–42).

The X chromosome encodes genes and proteins that participate in pathways that are disturbed in PH, such as inflammation, vascular remodelling, apoptosis, and reactive oxygen species production (43). Most of the X encoded genes are expressed equally in male and female cells because the second X chromosome in female cells is silenced by XIST, which is an X encoded long non-coding RNA (44). However, up to 30% of the second X chromosome genes escape inactivation, leading to a higher expression of these genes in female cells (1, 45, 46). Some of these genes escape X inactivation in all tissues, however, others are tissue specific (1, 47, 48). Sex differences might also arise due to XX mosaicism when there are polymorphisms that alter gene expression (43). If X chromosome inactivation randomly silences the paternal or maternal X chromosome in each cell, then in approximately 50% of cells in females the polymorphism producing higher expression of the gene will be present. This will lead to higher expression than in males whose single X chromosome has the more poorly expressing polymorphism. Despite these well-established mechanisms leading to differences in gene expression, the role of X chromosome encoded genes in sex differences in PH has not been widely studied.

We hypothesized that there are sex differences in the human pulmonary microvascular endothelium basally (in normoxia) and in response to hypoxia that are independent of differences in the sex hormone environment. Since endothelial cells constantly experience shear stress *in vivo*, HPMECs were cultured under physiological shear stress as described previously (49).

Methods

Cell culture

Human pulmonary microvascular endothelial cells (HPMECs) (Promocell, code C-12281) from healthy male and female donors were used. Female donors ranged in age from 53 to 70 years and male donors were 56-69 years old; all donors were Caucasian and non-smokers. Initially for omics analyses 3-4 donors were used and additional donors were added in other assays as they became available (see Appendix Table 1). HPMECs were grown in medium (MV2, Promocell) with Penicillin-Streptomycin 1% (Thermo Fisher Scientific) and supplements with serum 5% (code C-39226, Promocell). MV2 was used either with a low concentration of phenol red (3.3 µM) (code C-22221, Promocell) or without phenol red (code C-22226, Promocell). At passage five confluent HPMECs were exposed to physiological shear stress (mean shear stress was 13 dyn/cm^2) for 24 hours using an orbital shaker approach described previously (49). After 24 hours in these normoxic conditions, cells were either placed into hypoxic conditions (1% O_2 chamber, Coy Labs, Grass Lake, USA) or remained in normoxic conditions for a further 24 or 48 hours, while shear stress continued.

RNA sequencing

HPMECs were lysed in buffer RLT™ (Qiagen, Germantown, USA) with 1 M DTT (Merck, Darmstadt, Germany). Total RNA was extracted using spin columns (code 74104, RNeasy Mini Kit, Qiagen) with on-column DNAse treatment (code 79254, RNAse-Free DNase Set, Qiagen). Library Preparation and Sequencing were performed by Genewiz (Leipzig, Germany). RNA samples were quantified using Qubit 4.0 Fluorometer (Life Technologies, Carlsbad, CA, USA) and RNA integrity was checked with RNA Kit on Agilent 5300 Fragment Analyzer (Agilent Technologies, Palo Alto, CA, USA). All samples passed quality control. RNA sequencing library preparation was prepared using NEBNext Ultra II Directional RNA Library Prep Kit for Illumina following manufacturer's instructions (NEB, Ipswich, MA, USA). Sequencing libraries were validated using NGS Kit on the Agilent 5300 Fragment Analyzer (Agilent Technologies, Palo Alto, CA, USA), and quantified by using Qubit 4.0 Fluorometer (Invitrogen, Carlsbad, CA). The sequencing libraries were multiplexed and loaded on the flowcell on the Illumina NovaSeq 6000 instrument according to manufacturer's instructions. The samples were sequenced using a 2x150 Pair-End (PE) configuration v1.5. Image analysis and base calling were conducted by the NovaSeq Control Software v1.7 on the NovaSeq instrument. Raw sequence data (.bcl files) generated from Illumina NovaSeq was converted into fastq files and de-multiplexed using Illumina bcl2fastq program version 2.20. One mismatch was allowed for index sequence identification. After investigating the quality of the raw data, sequence reads were trimmed using Trimmomatic v.0.36 (50). The trimmed reads were mapped to the Homo sapiens reference genome available on ENSEMBL using the STAR aligner v.2.5.2b. BAM files were generated as a result of this step. Unique gene hit counts were calculated by using feature Counts from the Subread package v.1.5.2. Only unique reads that fell within exon

regions were counted. After extraction of gene hit counts, the gene hit counts table was used for downstream differential expression analysis. DESeq2 was used to identify differentially expressed genes (51).

Mass spectrometry-based proteomics

HPMECs were lysed, digested and purified using columns according to manufacturer's instruction (code P.O.00001, iST Sample Preparation Kit, PreOmics, Munich, Germany). The samples were analysed as a single batch by the Mass Spectrometry Resource (MSR) in University College Dublin on a hybrid quadrupole orbitrap mass spectrometer (Q Exactive, Thermo Scientific, Waltham, USA) connected to a chromatography system (Dionex Ultimate 3000, RSLCnano, Thermo Scientific, Waltham, USA) as previously described (49). Raw data from the mass spectrometer was processed using the MaxQuant software (version 2.0.3.0) incorporating the Andromeda search engine (52–54). To identify peptides and proteins, MS/MS spectra were matched against Uniprot homo sapiens database (2021_03) as previously described (49). Proteomics analysis was undertaken in Perseus software (version 1.6.2.3) according to developers protocol (55, 56). Protein abundances (label-free quantification, LFQ-intensities) were $\log_2$ transformed and only the proteins that were detected in at least two samples (out of three) in at least one group were kept. Missing (non-valid) values were replaced by imputing from a normal distribution (width 0.3, downshift 1.8 SD, separately for each column, e.g., sample) (55).

Gene Set Enrichment Analysis

Gene set enrichment analysis (GSEA, software version 4.1.0) was undertaken using normalised counts from the whole datasets (approximately 20 000 genes and 2900 proteins) (57). The Hallmark genet set collection was used, which includes 50 main cellular pathways (58). Pairwise comparisons were performed to identify sex different pathways (female samples were compared to male samples). For each pathway, the false discovery rate (FDR) was estimated using a permutation-based approach (1000 permutations for each gene set). The default settings used in GSEA were permutation-based FDR (1000 permutations), type "gene_set" (randomisation of genes), gene set size range was from 15 to 500 genes. Gene sets (pathways) were considered statistically significantly enriched if the FDR q value was less than 0.05. Venn diagrams were used (Venny 2.1 online tool (59) to demonstrate pathways that were enriched (FDR q value<0.05) in female or male HPMECs according to RNA sequencing and proteomics analyses.

Real time qPCR

Total RNA (1 µg) was used for reverse transcription (code 18080-044, SuperScript™ III, Invitrogen). RT-qPCR was undertaken using TaqMan® assays (4331182, Thermo Scientific, Waltham, USA): THBS1 (Hs00962908_m1) and MMP2 (Hs01548727_m1). Analysis of RT-qPCR data was performed using the standard curve method. Target gene expression was normalized to ACTB (Hs01060665_g1).

Western blotting

HPMECs were lysed in RIPA buffer (code 89900, Pierce™, Thermo Scientific). The protein lysates were centrifuged at 16 000 g at 4°C for 15 minutes and the supernatant was collected. The protein concentration was measured using BCA protein assay (code 23225, Pierce™, Thermo Scientific). 12 µg of protein was mixed with LDS Sample Loading Buffer (4X) (G-

Biosciences, St. Louis, USA) and Bolt™ Sample Reducing Agent (10X) (Invitrogen, Waltham, USA) and incubated at 70°C for 10 minutes for denaturation. Electrophoresis, transfer and immunodetection were undertaken as previously described (49). Primary antibodies against Thrombospondin-1 (1:10000, rabbit monoclonal, D7E5F, #37879, lot1, 37879d, Cell Signaling, (60)) and β-actin (1:5000, mouse monoclonal, A5441, lot 029M4883V, Merck, Darmstadt, Germany) were used. The secondary antibodies used were as follows: goat anti-rabbit IgG (1:5000, DyLight™ 800, SA535571, lot TL277458, Invitrogen, Waltham, USA) and goat anti-mouse IgG (1:1000, DyLight™ 680, 35519, lot VB298075, Invitrogen, Waltham, USA). Thrombospondin 1 protein expression was normalised to β-actin from the same sample.

Proliferation assay

Cell proliferation rate was assessed using Click-iT® Plus EdU Cell Proliferation Kit for Imaging (C10640, Invitrogen, Thermo Scientific). After 24 hours of hypoxia (or normoxia as control) HPMECs were incubated with EdU for three hours in hypoxia (or normoxia). HPMECs were stained and imaged according to the supplier's protocol and the ratio of new to old nuclei was compared between the sexes. Images were taken at 10x magnification using an inverted Zeiss Axiovert 200 microscope (Carl Zeiss) along a central diameter of a well (27 images per well). Nuclei were counted using Imaris x64 7.6.5, function "Spots". Numbers of all nuclei and new nuclei were recorded. The ratio of new nuclei to all nuclei was calculated for each image and averaged for each well.

Tube formation assay

Tube formation assay was undertaken to examine how male and female HPMECs form capillary-like structures (61, 62). Ibidi µ-slides Angiogenesis were used (cat. No 81506, Ibidi, Munich, Germany). Each well was precoated with 10 µl of Matrigel® (phenol-red free, lot 1069003, ref 356237, Corning, Bedford, MA USA). HPMECs at passage 5 were seeded (10 000 cells/well) with 50 µl/well of standard MV2 medium with supplements, Promocell, Heidelberg, Germany). For technical replicates five wells were used for one donor in one experimental condition (normoxia or hypoxia). HPMECs in µ-slides were incubated in a standard TC incubator (normoxia) or in hypoxia (1% O_2) for five hours. Images of tubes were taken using an inverted phase-contrast microscope (CKX53, Olympus) at 4x magnification (one image per well). Tube formation was analysed using a commercial web-based software FastTrack AI (Metavì labs, Ibidi, Munich, Germany) that reports loop count, average loop area, average tube length (per loop), total tube length and branch count. Resolution of the images was 0.715 pixels/µm. Before analysis images were cropped in ImageJ (63) to remove areas where no Matrigel® was present (outside the well). The final area of a cropped image was measured in ImageJ. Values reported by FastTrack AI were normalised per area of an analysed image.

Statistical analysis

To display differences in the expression of individual RNAs and proteins between males and females, volcano plots were used. Differentially expressed RNAs were identified by pairwise comparisons using a P value <0.05 following adjustment for multiple comparisons (Wald test with Benjamini-Hochberg correction). On the volcano plots showing proteomics data an uncorrected P value ($P < 0.05$, T test) is shown for illustrative purposes because no differentially expressed proteins were identified following adjustment for multiple comparisons. For the GSEA FDR, a q value <0.05 (permutation-based FDR, 1000

permutations) was accepted as significant. For other assays (proliferation assay, RT-qPCR and western blotting), a P value <0.05 (T test, GraphPad Prism 9, San Diego, USA) was accepted as indicating a statistically significant difference.

Results

Sex different genes and proteins

Differentially expressed genes (DEGs) in male and female HPMECs, cultured in normoxia or hypoxia, were identified (Figure 1A-1D, Appendix Tables 2-5). The most striking difference was detected in the expression of Y-chromosome encoded genes (varying between 11 and 12 depending on the condition), including a number of genes previously identified as potentially playing a role in the development of pulmonary hypertension, RPS4Y1, DDX3Y, UTY, ZFY and PRKY (Figures 1A-D) (34, 35). Of note, the Y chromosome encoded gene SRY has not been detected in either male or female HPMECs. As expected, among the X-encoded genes the most striking sex difference was found in XIST expression, which was expressed more highly in female HPMECs than in male HPMECs (Figures 1A-D). A small number of other X-encoded genes (KLHL13, RPS4X, SLC6A8 and NRK) were expressed more highly in female cells than in male cells (p adj<0.05) (Fig 1A-D). The proteomics datasets were explored to specifically examine the expression of the proteins encoded by the differentially expressed genes located on the sex chromosomes. None of the proteins encoded by the differentially expressed mRNAs whose genes were located on the Y chromosome were detected in the proteomics analysis (Figure 1E-1H, Appendix Tables 6-9). Among the four genes located on the X chromosome (KLHL13, RPS4X, SLC6A8 and NRK) that were expressed more highly in female HPMECs, only one corresponding protein (RPS4X, 40S ribosomal protein S4, X isoform) was detected by proteomics analysis and it was not differentially expressed between male and female HPMECs.

No proteins were identified as differentially expressed between females and male datasets when using a P value adjusted for multiple comparisons (Figure 1E-1H, Appendix Tables 6-9). Interestingly, even with a less stringent threshold in the proteomics data (unadjusted P <0.05), only a small number of differentially expressed genes and proteins overlapped (Appendix Figure 1). This led us to explore the omics datasets using an additional analysis approach, Gene Set Enrichment Analysis (GSEA).

Sex different pathways

Gene Set Enrichment Analysis (GSEA) was used to identify gene sets (pathways) that were enriched in one sex compared to another sex in both transcriptomic and proteomics datasets (Figure 2). This approach analyses the whole dataset, i.e. it does not require splitting the data into significantly changed and unchanged genes or proteins (57). Hence, it allows inclusion of all genes or proteins in the analysis and not only those that reached a specific fold-change or p-value.

In the RNA sequencing dataset following 24 hours of normoxia, 13 gene sets were enriched in female HPMECs, and three gene sets were enriched in male HPMECs (Figure 2A). In response to 24 hours of hypoxia, 20 gene sets were enriched in female HPMECs, and two gene sets were enriched in male HPMECs (Figure 2C). In response to 48 hours of normoxia eight gene sets were enriched in female HPMEC, and three gene sets were enriched in male

HPMECs (Figure 2E). In response to 48 hours of hypoxia 19 gene sets were enriched in female HPMECs, and two gene sets were enriched in male HPMECs (Figure 2G). Fewer pathways were enriched (FDR q value<0.05) in the proteomics datasets compared to the RNA sequencing datasets (Figure 2B, 2D, 2F, 2H).

Overlapping pathways on RNA and protein levels

To display pathways that were consistently enriched in one sex relative to the other in both RNA sequencing and proteomics datasets, Venn diagrams were used (Figures 3-5). When a specific pathway was enriched in both RNA sequencing and proteomics analyses, the top ten leading-edge genes and proteins, which influenced pathway enrichment the most, are presented in each of the Venn diagrams (Figures 3-5).

Pathways enriched in female HPMECs in normoxia (Figure 3) are presented separately from pathways enriched in female HPMECs in hypoxia (Figure 4). The epithelial to mesenchymal transition pathway was enriched in female HPMECs in both RNA sequencing and proteomics datasets in both normoxia and hypoxia at both time points (Figures 3 and 4). Pathways enriched in male HPMECs in normoxia are shown in Figure 5. Two pathways (G2M checkpoint and E2F targets) were enriched in the RNA sequencing datasets from male HPMECs following 24 and 48 hours of hypoxia, both of which are concerned with the regulation of cell proliferation (64) (Figure 5). In the proteomics datasets, one of these two pathways (E2F targets) was enriched in normoxia at both 24 and 48 hours, while the G2M Checkpoint pathway was enriched in both datasets at 48 hours of normoxia (Figure 5). No pathways were enriched in the proteomics datasets from male HMPECs following either 24 or 48 hours of hypoxia (Figure 2D and 2H); hence, there was no overlap between RNA and protein pathways (Venn diagrams not shown). Some pathways overlapped between the two hypoxia duration times (24 and 48 hours) reflecting a more sustained and prolonged sex difference.

Pathways that were enriched on the protein level were in a good agreement with pathways that were enriched on the RNA level. Interestingly, even when the same pathway was enriched in both RNA sequencing and proteomics datasets at the same time point, the 10 leading-edge genes and proteins (i.e. those that influenced pathway enrichment the most) were not identical in the two datasets. This supports an approach of integrating omics data based on pathways, rather than looking at individual genes and proteins. Two pathways that regulate proliferation were enriched in male HPMECs on RNA and protein levels, G2M checkpoint and E2F targets (64) (Figure 5).

***In vitro* assays of specific pathways, genes and proteins**

Because of the enrichment of pathways involved in proliferation (G2M Checkpoint and E2F targets) in male HMPECs, we compared proliferation rates in male and female HPMECs in normoxia and hypoxia *in vitro* in a further series of experiments (Figures 6A-6D). Male HPMECs had a higher proliferation rate in normoxia than female HPMECs (Figure 6C). There was no statistically significant difference between male and female HPMEC proliferation rate in hypoxia (Figure 6D). Angiogenesis, a pathway enriched in female cells in normoxia and hypoxia at both 24 and 48 hours in RNA sequencing datasets (Figures 2A, 2C, 2E, 2G), is of direct relevance to the development of pulmonary hypertension so we also assessed it *in vitro* using a tube formation assay. No differences in tube formation were detected between male and female HPMECs in normoxia or hypoxia (Appendix Figure 2).

Given the higher rate of proliferation observed in male HMPECs, it was interesting to note that among the leading-edge genes in the epithelial to mesenchymal transition pathway was a well-known inhibitor of proliferation, thrombospondin 1 (65). Using RT-qPCR and Western blotting we confirmed that thrombospondin 1 was more highly expressed in female HPMECs than in male HPMECs in normoxia (Figure 6E and 6G and Appendix Figure 3).

Discussion

The current study demonstrated for the first time sex dependent differences in cellular pathways in pulmonary microvascular endothelial cells both in normoxia and hypoxia. Pathways known to regulate cell proliferation were persistently enriched in male cells in both normoxia and hypoxia. The functional importance of this was demonstrated in further experiments *in vitro* in which we found that male cells had a higher rate of proliferation in normoxic conditions than female cells. Importantly, these sex differences were detected in HPMECs that were cultured in the absence of sex hormones. To our knowledge, this study is the first to demonstrate sex differences in human pulmonary endothelial cells from the microvasculature, the major site of the pulmonary vascular remodelling that underlies the progressive increase in vascular resistance in pulmonary hypertension (17, 66, 67).

As expected, Y- and X-chromosome encoded genes were among the sex different genes detected in HPMECs. We found that the Y-encoded gene UTY was highly expressed in male HPMECs and, interestingly, this gene has previously been implicated in the sexual dimorphism in pulmonary hypertension (34, 35). UTY expression in the lungs of male mice exposed to hypoxia reduced pulmonary arterial pressure when compared to female mice and siRNA mediated knockdown of UTY in the male mice increased the pulmonary hypertensive response to hypoxia (35). The anti-hypertensive effect of Uty was largely mediated by its anti-inflammatory action suppressing CXCL9 and CXCL10 secretion (35). Interestingly, in male patients with pulmonary arterial hypertension, UTY expression is reduced in lung tissue compared to healthy male controls (34). Our results align well with these previous findings and identify the pulmonary microvascular endothelium as an important site of UTY expression in humans. A second Y-encoded gene, SRY, has previously been reported as having a potential role in protection against pulmonary hypertension in males due to its ability to induce BMPR2 expression in dermal fibroblasts (37). Curiously, its expression was not detected in lung tissue (35, 37), which is in keeping with our findings reported here that SRY was not expressed in human pulmonary microvascular endothelial cells. Thus, the role of this gene in pulmonary hypertension remains to be elucidated.

The X chromosome encoded long non-coding RNA, XIST, was expressed more highly in female HPMECs than in male HPMECs. The canonical role of XIST is to silence gene expression on the second X chromosome in female cells (44), however, XIST can also regulate expression of X encoded transcription factors that might affect expression of autosomal genes (20). Other X encoded long non-coding RNAs and microRNAs can also regulate autosomal gene expression (43). These non-coding RNAs may account for some of the differences observed between male and female cells if they were expressed more highly in female cells due to their escape from X chromosome inactivation (24). Here we have detected a number of genes (KLHL13, RPS4X, SLC6A8 and NRK) that might be potential X chromosome inactivation escapees, however, their roles in the development of PH have not been studied.

GSEA identified enrichment of pathways in female endothelial cells in the absence of sex hormone differences that were present either basally (in normoxia) or in hypoxia and may therefore contribute to the sex differences in PH. These included pathways that are known to be important in the development of PH in female endothelial cells including TGF-β signalling (68), inflammatory responses (69, 70), coagulation (71) and epithelial-to-mesenchymal transition (72). Interestingly, two pathways that are involved in cellular proliferation (G2M checkpoint, and E2F targets (64)) were enriched in male HPMECs in normoxia in both the RNA and proteomics datasets. In support of these findings, we found that the proliferation rate was also higher in male HPMECs *in vitro*. A higher proliferation rate of male pulmonary endothelial cells has been shown previously in murine lung endothelial cells (MLEC) and in pulmonary endothelial cells in large conduit arteries (25, 33). Our data show that higher proliferation rate is also a feature of the pulmonary microvascular endothelial cells, which is of particular interest as the microvasculature is the site of the vascular remodelling that causes the development of pulmonary hypertension. It is not clear how increased proliferation of male HPMECs could account for the differences in incidence and prognosis of PH between males and females. Despite their better prognosis, female patients with pulmonary hypertension caused by hypoxia in chronic lung diseases have higher pulmonary vascular resistance than males (13, 73). Lower proliferation rates in female HPMECs in normoxia might predispose females to higher pulmonary vascular resistance in PH if it reduces the capacity for endothelial repair and vascular homeostasis, processes that are known to attenuate PH (74–76). The role of differences in proliferation rates between male and female HPMECs requires further exploration in future studies.

Despite the enrichment of the angiogenesis pathway in female HPMECs on the RNA level, no sex differences were detected in the tube formation assay *in vitro*. An important limitation of this *in vitro* approach is that endothelial cells do not proliferate in this assay (62). Hence, even though the tube formation assay is a commonly used way to study angiogenesis *in vitro*, it does not fully recapitulate angiogenesis *in vivo*.

Thrombospondin-1 (THBS1) was among the proteins that were expressed more highly in female HPMECs compared to male HPMECs. This finding was notable since THBS1 plays an important role in the development of PH. THBS1 inhibits eNOS signalling and has been found to be elevated in pulmonary arteries and in the plasma of patients with PH (77–81). Moreover, 5-year mortality of patients with PH positively correlated with THBS1 plasma concentrations (81). THBS1 has been shown to inhibit endothelial cell proliferation, hence, it could contribute to the lower proliferation rate of female HPMECs that we observed (65). It is worth noting that we have previously shown that THBS1 is hypoxia-responsive only when pulmonary microvascular endothelial cells are exposed to physiological shear stress but not when cells are cultured under static conditions (49). Taken together with the results reported here, this suggests that cells should be studied under conditions that reproduce the shear stress present *in vivo* in order to yield insights of relevance to the regulation of endothelial cell behaviour in the hypoxic lung in vivo.

Culturing of cells isolated from male and female donors in the absence of the sex hormones is a straightforward model for investigating the sex chromosomal influence on the sex differences, however, this method does not allow complete elimination of the impact of the sex hormones. Sex hormones have a long-lasting programming effect on cells (82) and the absence of the sex hormones can only eliminate the acute actions of differences in the sex hormone environment to which the cells were exposed prior to isolation. Information about

the circulating hormone concentrations of the donors, whose HMPECs were used in this study, was not available. Importantly, in the study reported here, HPMECs from both sexes were cultured in identical medium and thus the acute effects of differences in sex hormone concentration were eliminated.

Although our findings show that there are differences between male and female endothelial cells that are independent of sex hormones, the sample size was relatively small and should be increased in future studies. In addition, subjects beyond those solely of the Caucasian backgrounds included in this report should be added which would increase the relevance of their results to a broader range of populations. Confirmation studies in lungs of female and male patients with pulmonary hypertension are also needed to determine which of the pathways identified in our *in vitro* studies are directly relevant to *in vivo* conditions and therefore might be used as novel therapeutic targets. These targets may ultimately facilitate the development of sex specific therapies for pulmonary hypertension.

The work presented here reveals for the first time that human female and male pulmonary microvascular endothelial cells, cultured in conditions of physiological shear stress, express different RNAs and proteins basally and in hypoxia. Given that remodelling of the pulmonary microvasculature is the primary cause of the increased vascular resistance driving the development of pulmonary hypertension, the identified sex differences might contribute to the sexual dimorphism observed in pulmonary hypertension and require further investigation.

Data availability

Gene expression profiling data were deposited in National Center of Biotechnology Information's Gene Expression Omnibus (GEO) and are accessible through GEO Series accession number GSE233547. The mass spectrometry proteomics data have been deposited to the ProteomeXchange Consortium via the PRIDE partner repository. Project accession: PXD046787, Project

DOI: https://doi.org/10.6019/PXD046787.

Supplemental data

Supplemental data for Figure 6 and Supplemental data for Appendix Figure 2:

DOI https://doi.org/10.6084/m9.figshare.24496270

Acknowledgements

The authors thank Dr. Dimitri Scholz for help with imaging.

Grants

UCD internal funding

Disclosures

None

Disclaimers

None

Author contributions

DSK, PMcL conceived and designed research. DSK, NVP, AJ, ED performed experiments. DSK, NVP, AJ, ED, PMcL analyzed data. DSK, NVP, AJ, ED, JAB, PMcL Interpreted results of experiments. DSK, NVP, AJ, ED prepared figures. DSK, PMcL drafted manuscript. DSK, NVP, AJ, PMcL edited and revised manuscript. DSK, NVP, AJ, ED, JAB, PMcL Approved final version of manuscript.

Appendix

References

1. **Oliva M**, **Muñoz-Aguirre M**, **Kim-Hellmuth S**, **Wucher V**, **Gewirtz ADH**, **Cotter DJ**, **Parsana P**, **Kasela S**, **Balliu B**, **Viñuela A**, **Castel SE**, **Mohammadi P**, **Aguet F**, **Zou Y**, **Khramtsova EA**, **Skol AD**, **Garrido-Martín D**, **Reverter F**, **Brown A**, **Evans P**, **Gamazon ER**, **Payne A**, **Bonazzola R**, **Barbeira AN**, **Hamel AR**, **Martinez-Perez A**, **Soria JM**, **Pierce BL**, **Stephens M**, **Eskin E**, **Dermitzakis ET**, **Segrè A V.**, **Im HK**, **Engelhardt BE**, **Ardlie KG**, **Montgomery SB**, **Battle AJ**, **Lappalainen T**, **Guigó R**, **Stranger BE**. The impact of sex on gene expression across human tissues. *Science (80-)* 369, 2020. doi: 10.1126/science.aba3066.

2. **Regitz-Zagrosek V**, **Kararigas G**. Mechanistic pathways of sex differences in cardiovascular disease. *Physiol Rev* 97: 1–37, 2017. doi: 10.1152/physrev.00021.2015.

3. **Werner RJ**, **Schultz BM**, **Huhn JM**, **Jelinek J**, **Madzo J**, **Engel N**. Sex chromosomes drive gene expression and regulatory dimorphisms in mouse embryonic stem cells. *Biol Sex Differ* 8: 1–18, 2017. doi: 10.1186/s13293-017-0150-x.

4. **Klein SL**, **Flanagan KL**. Sex differences in immune responses. *Nat Rev Immunol* 16: 626–638, 2016. doi: 10.1038/nri.2016.90.

5. **Arnold AP**. Sexual differentiation of brain and other tissues: Five questions for the next 50 years. *Horm Behav* 120: 104691, 2020. doi: 10.1016/j.yhbeh.2020.104691.

6. **Han MK**, **Arteaga-Solis E**, **Blenis J**, **Bourjeily G**, **Clegg DJ**, **DeMeo D**, **Duffy J**, **Gaston B**, **Heller NM**, **Hemnes A**, **Jain R**, **Henske EP**, **Lahm T**, **Lancaster LH**, **Lee J**, **Legato MJ**, **McKee S**, **Mehra R**, **Morris A**, **Prakash YS**, **Stampfli MR**, **Gopal-Srivastava R**, **Punturieri ADLA**, **Reineck L**, **Tigno X**, **Clayton J**. Female Sex and Gender in Lung/Sleep Health and Disease: Increased Understanding of Basic Biological, Pathophysiological and Behavioral Mechanisms Leading to Better Health for Female Patients with Lung Disease. *Am J Respir Crit Care Med* 198: 850–858, 2018.

7. **Humbert M**, **Kovacs G**, **Hoeper MM**, **Badagliacca R**, **Berger RMF**, **Brida M**, **Carlsen J**, **Coats AJS**, **Escribano-Subias P**, **Ferrari P**, **Ferreira DS**, **Ghofrani HA**, **Giannakoulas G**, **Kiely DG**, **Mayer E**, **Meszaros G**, **Nagavci B**, **Olsson KM**, **Pepke-Zaba J**, **Quint JK**, **Rådegran G**, **Simonneau G**, **Sitbon O**, **Tonia T**, **Toshner M**, **Vachiery J-L**, **Noordegraaf AV**, **Delcroix M**, **Rosenkranz S**. 2022 ESC/ERS Guidelines for the diagnosis and treatment of pulmonary hypertension. *Eur Heart J* 43: 3618–3731, 2022.

8. **Humbert M**, **Sitbon O**, **Chaouat A**, **Bertocchi M**, **Habib G**, **Gressin V**, **Yaïci A**, **Weitzenblum E**, **Cordier JF**, **Chabot F**, **Dromer C**, **Pison C**, **Reynaud-Gaubert M**, **Haloun A**, **Laurent M**, **Hachulla E**, **Cottin V**, **Degano B**, **Jaïs X**, **Montani D**, **Souza R**, **Simonneau G**. Survival in patients with idiopathic, familial, and anorexigen-associated pulmonary arterial hypertension in the modern management era. *Circulation* 122: 156–163, 2010. doi: 10.1161/CIRCULATIONAHA.109.911818.

9. **Girerd B**, **Montani D**, **Eyries M**, **Yaici A**, **Sztrymf B**, **Coulet F**, **Sitbon O**, **Simonneau G**, **Soubrier F**, **Humbert M**. Absence of influence of gender and BMPR2 mutation type on

clinical phenotypes of pulmonary arterial hypertension. *Respir Res* 11, 2010. doi: 10.1186/1465-9921-11-73.

10. **McGoon MD**, **Benza RL**, **Escribano-Subias P**, **Jiang X**, **Miller DP**, **Peacock AJ**, **Pepke-Zaba J**, **Pulido T**, **Rich S**, **Rosenkranz S**, **Suissa S**, **Humbert M**. Pulmonary arterial hypertension: Epidemiology and registries. *J Am Coll Cardiol* 62, 2013. doi: 10.1016/j.jacc.2013.10.023.

11. **Hester J**, **Ventetuolo C**, **Lahm T**. Sex, Gender, and Sex Hormones in Pulmonary Hypertension and Right Ventricular Failure. *Compr Physiol* 10: 125–170, 2019. doi: 10.1002/cphy.c190011.Sex.

12. **Melenovsky V**, **Hwang SJ**, **Lin G**, **Redfield MM**, **Borlaug BA**. Right heart dysfunction in heart failure with preserved ejection fraction. *Eur Heart J* 35: 3452–3462, 2014. doi: 10.1093/eurheartj/ehu193.

13. **Prins KW**, **Rose L**, **Archer SL**, **Pritzker M**, **Weir EK**, **Olson MD**, **Thenappan T**. Clinical determinants and prognostic implications of right ventricular dysfunction in pulmonary hypertension caused by chronic lung disease. *J Am Heart Assoc* 8: 1–15, 2019. doi: 10.1161/JAHA.118.011464.

14. **Rodriguez-Arias JJ**, **García-Álvarez A**. Sex Differences in Pulmonary Hypertension. *Front Aging* 2: 1–11, 2021. doi: 10.3389/fragi.2021.727558.

15. **Frump AL**, **Albrecht M**, **Yakubov B**, **Breuils-Bonnet S**, **Nadeau V**, **Tremblay E**, **Potus F**, **Omura J**, **Cook T**, **Fisher A**, **Rodriguez B**, **Brown RD**, **Stenmark KR**, **Rubinstein CD**, **Krentz K**, **Tabima DM**, **Li R**, **Sun X**, **Chesler NC**, **Provencher S**, **Bonnet S**, **Lahm T**. 17β-estradiol and estrogen receptor-α protect right ventricular function in pulmonary hypertension via BMPR2 and apelin. *J Clin Invest* 131: e129433, 2021.

16. **Hester J**, **Ventetuolo C**, **Lahm T**. Sex, gender, and sex hormones in pulmonary hypertension and right ventricular failure. *Compr Physiol* 10: 125–170, 2020. doi: 10.1002/cphy.c190011.

17. **Costello CM**, **Howell K**, **Cahill E**, **McBryan J**, **Konigshoff M**, **Eickelberg O**, **Gaine S**, **Martin F**, **McLoughlin P**. Lung-selective gene responses to alveolar hypoxia: potential role for the bone morphogenetic antagonist gremlin in pulmonary hypertension. *Am J Physiol Cell Mol Physiol* 295: L272–L284, 2008. doi: 10.1152/ajplung.00358.2007.

18. **Stenmark KR**, **Fagan KA**, **Frid MG**. Hypoxia-induced pulmonary vascular remodeling: Cellular and molecular mechanisms. *Circ Res* 99: 675–691, 2006. doi: 10.1161/01.RES.0000243584.45145.3f.

19. **Hayward-Piatkovskyi B**, **Gonyea CR**, **Pyle SC**, **Lingappan K**, **Gleghorn JP**. Sex-related external factors influence pulmonary vascular angiogenesis in a sex-dependent manner. *Am J Physiol - Hear Circ Physiol* 324: H26–H32, 2023. doi: 10.1152/ajpheart.00552.2022.

20. **Qin S**, **Predescu DN**, **Patel M**, **Drazkowski P**, **Ganesh B**, **Predescu SA**. Sex differences in the proliferation of pulmonary artery endothelial cells: Implications for plexiform arteriopathy. *J Cell Sci* 133, 2020. doi: 10.1242/jcs.237776.

21. **Du L**, **Bayir H**, **Lai Y**, **Zhang X**, **Kochanek PM**, **Watkins SC**, **Graham SH**, **Clark RSB**.

Innate gender-based proclivity in response to cytotoxicity and programmed cell death pathway. *J Biol Chem* 279: 38563–38570, 2004. doi: 10.1074/jbc.M405461200.

22. **Du L**, **Hickey RW**, **Bayir H**, **Watkins SC**, **Tyurin VA**, **Guo F**, **Kochanek PM**, **Jenkins LW**, **Ren J**, **Gibson G**, **Chu CT**, **Kagan VE**, **Clark RSB**. Starving neurons show sex difference in autophagy. *J Biol Chem* 284: 2383–2396, 2009. doi: 10.1074/jbc.M804396200.

23. **Lefèvre N**, **Corazza F**, **Valsamis J**, **Delbaere A**, **De Maertelaer V**, **Duchateau J**, **Casimir G**. The number of X chromosomes influences inflammatory cytokine production following Toll-like receptor stimulation. *Front Immunol* 10, 2019. doi: 10.3389/fimmu.2019.01052.

24. **Matarrese P**, **Tieri P**, **Anticoli S**, **Ascione B**, **Conte M**, **Franceschi C**, **Malorni W**, **Salvioli S**, **Ruggieri A**. X-chromosome-linked miR548am-5p is a key regulator of sex disparity in the susceptibility to mitochondria-mediated apoptosis. *Cell Death Dis* 10, 2019. doi: 10.1038/s41419-019-1888-3.

25. **Zemskova M**, **Kurdyukov S**, **James J**, **McClain N**, **Rafikov R**, **Rafikova O**. Sex-specific stress response and HMGB1 release in pulmonary endothelial cells. *PLoS One* 15: e0231267, 2020. doi: 10.1371/journal.pone.0231267.

26. **Zhang Y**, **Dong X**, **Shirazi J**, **Gleghorn JP**, **Lingappan K**. Pulmonary endothelial cells exhibit sexual dimorphism in their response to hyperoxia. *Am J Physiol - Hear Circ Physiol* 315: H1287–H1292, 2018. doi: 10.1152/ajpheart.00416.2018.

27. **Addis R**, **Campesi I**, **Fois M**, **Capobianco G**, **Dessole S**, **Fenu G**, **Montella A**, **Cattaneo MG**, **Vicentini LM**, **Franconi F**. Human umbilical endothelial cells (HUVECs) have a sex: Characterisation of the phenotype of male and female cells. *Biol Sex Differ* 5: 1–12, 2014. doi: 10.1186/s13293-014-0018-2.

28. **Lorenz M**, **Koschate J**, **Kaufmann K**, **Kreye C**, **Mertens M**, **Kuebler WM**, **Baumann G**, **Gossing G**, **Marki A**, **Zakrzewicz A**, **Miéville C**, **Benn A**, **Horbelt D**, **Wratil PR**, **Stangl K**, **Stangl V**. Does cellular sex matter? Dimorphic transcriptional differences between female and male endothelial cells. *Atherosclerosis* 240: 61–72, 2015. doi: 10.1016/j.atherosclerosis.2015.02.018.

29. **Lorenz M**, **Blaschke B**, **Benn A**, **Hammer E**, **Witt E**, **Kirwan J**, **Fritsche-Guenther R**, **Gloaguen Y**, **Bartsch C**, **Vietzke A**, **Kramer F**, **Kappert K**, **Brunner P**, **Nguyen HG**, **Dreger H**, **Stangl K**, **Knaus P**, **Stangl V**. Sex-specific metabolic and functional differences in human umbilical vein endothelial cells from twin pairs. *Atherosclerosis* 291: 99–106, 2019. doi: 10.1016/j.atherosclerosis.2019.10.007.

30. **Witt E**, **Lorenz M**, **Völker U**, **Stangl K**, **Hammer E**, **Stangl V**. Sex-specific differences in the intracellular proteome of human endothelial cells from dizygotic twins. *J Proteomics* 201: 48–56, 2019. doi: 10.1016/j.jprot.2019.03.016.

31. **Wang J**, **Bingaman S**, **Huxley VH**. Intrinsic sex-specific differences in microvascular endothelial cell phosphodiesterases. *Am J Physiol - Hear Circ Physiol* 298: 1146–1154, 2010. doi: 10.1152/ajpheart.00252.2009.

32. **Deasy BM**, **Lu A**, **Tebbets JC**, **Feduska JM**, **Schugar RC**, **Pollett JB**, **Sun B**, **Urish KL**, **Gharaibeh BM**, **Cao B**, **Rubin RT**, **Huard J**. A role for cell sex in stem cell-mediated

skeletal muscle regeneration: Female cells have higher muscle regeneration efficiency. *J Cell Biol* 177: 73–86, 2007. doi: 10.1083/jcb.200612094.

33. **Cox-Flaherty K**, **Baird GL**, **Braza J**, **Guarino BD**, **Princiotto A**, **Ventetuolo CE**, **Harrington EO**. Commercial human pulmonary artery endothelial cells have in-vitro behavior that varies by sex. *Pulm Circ* 12: 1–9, 2022. doi: 10.1002/pul2.12165.

34. **Umar S**, **Cunningham CM**, **Itoh Y**, **Moazeni S**, **Vaillancourt M**, **Sarji S**, **Centala A**, **Arnold AP**, **Eghbali M**. The Y Chromosome Plays a Protective Role in Experimental Hypoxic Pulmonary Hypertension. *Am J Respir Crit Care Med* 197: 952–955, 2018.

35. **Cunningham CM**, **Li M**, **Ruffenach G**, **Doshi M**, **Aryan L**, **Hong J**, **Park J**, **Hrncir H**, **Medzikovic L**, **Umar S**, **Arnold AP**, **Eghbali M**. Y-Chromosome Gene, Uty, Protects Against Pulmonary Hypertension by Reducing Proinflammatory Chemokines. *Am J Respir Crit Care Med* 206: 186–196, 2022.

36. **Predescu DN**, **Mokhlesi B**, **Predescu SA**. The Impact of Sex Chromosomes in the Sexual Dimorphism of Pulmonary Arterial Hypertension. *Am J Pathol* 192: 582–594, 2022. doi: 10.1016/j.ajpath.2022.01.005.

37. **Yan L**, **Cogan J**, **Hedges L**, **Nunley B**, **Hamid R**, **Austin E**. The Y Chromosome Regulates BMPR2 Expression Via SRY: A Possible Reason 'Why' Fewer Males Develop PAH. .

38. **Meng L**, **Teng X**, **Liu Y**, **Yang C**, **Wang S**, **Yuan W**, **Meng J**, **Chi H**, **Duan L**, **Liu X**. Vital Roles of Gremlin-1 in Pulmonary Arterial Hypertension Induced by Systemic-to-Pulmonary Shunts. *J Am Heart Assoc* 9: e016586, 2020. doi: 10.1161/JAHA.120.016586.

39. **Barnes JW**, **Kucera ET**, **Tian L**, **Mellor NE**, **Dvorina N**, **Baldwin WW**, **Aldred MA**, **Farver CF**, **Comhair SAA**, **Aytekin M**, **Dweik RA**. Bone morphogenic protein type 2 receptor mutation-independent mechanisms of disrupted bone morphogenetic protein signaling in idiopathic pulmonary arterial hypertension. *Am J Respir Cell Mol Biol* 55: 564–575, 2016. doi: 10.1165/rcmb.2015-0402OC.

40. **Cahill E**, **Costello CM**, **Rowan SC**, **Harkin S**, **Howell K**, **Leonard MO**, **Southwood M**, **Cummins EP**, **Fitzpatrick SF**, **Taylor CT**, **Morrell NW**, **Martin F**, **McLoughlin P**. Gremlin plays a key role in the pathogenesis of pulmonary hypertension. *Circulation* 125: 920–930, 2012. doi: 10.1161/CIRCULATIONAHA.111.038125.

41. **Austin ED**, **Loyd JE**. The Genetics of Pulmonary Arterial Hypertension. *Circ Res* 115: 189–200, 2014. doi: 10.1016/j.gaitpost.2006.08.001.

42. **Johnson JA**, **Hemnes AR**, **Perrien DS**, **Schuster M**, **Robinson LJ**, **Gladson S**, **Loibner H**, **Bai S**, **Blackwell TR**, **Tada Y**, **Harral JW**, **Talati M**, **Lane KB**, **Fagan KA**, **West J**. Cytoskeletal defects in Bmpr2-associated pulmonary arterial hypertension. *Am J Physiol - Lung Cell Mol Physiol* 302: 474–484, 2012. doi: 10.1152/ajplung.00202.2011.

43. **Kostyunina DS**, **McLoughlin P**. Sex dimorphism in pulmonary hypertension: The role of the sex chromosomes. *Antioxidants* 10, 2021. doi: 10.3390/antiox10050779.

44. **Snell DM**, **Turner JMA**. Sex Chromosome Effects on Male – Female Differences in Mammals. *Curr Biol* 28: R1313–R1324, 2018. doi: 10.1016/j.cub.2018.09.018.

45. **Tukiainen T**, **Villani AC**, **Yen A**, **Rivas MA**, **Marshall JL**, **Satija R**, **Aguirre M**, **Gauthier L**, **Fleharty M**, **Kirby A**, **Cummings BB**, **Castel SE**, **Karczewski KJ**, **Aguet F**, **Byrnes A**, **Gelfand ET**, **Getz G**, **Hadley K**, **Handsaker RE**, **Huang KH**, **Kashin S**, **Lek M**, **Li X**, **Nedzel JL**, **Nguyen DT**, **Noble MS**, **Segrè A V.**, **Trowbridge CA**, **Abell NS**, **Balliu B**, **Barshir R**, **Basha O**, **Battle A**, **Bogu GK**, **Brown A**, **Brown CD**, **Chen LS**, **Chiang C**, **Conrad DF**, **Cox NJ**, **Damani FN**, **Davis JR**, **Delaneau O**, **Dermitzakis ET**, **Engelhardt BE**, **Eskin E**, **Ferreira PG**, **Frésard L**, **Gamazon ER**, **Garrido-Martín D**, **Gewirtz ADH**, **Gliner G**, **Gloudemans MJ**, **Guigo R**, **Hall IM**, **Han B**, **He Y**, **Hormozdiari F**, **Howald C**, **Im HK**, **Jo B**, **Kang EY**, **Kim Y**, **Kim-Hellmuth S**, **Lappalainen T**, **Li G**, **Li X**, **Liu B**, **Mangul S**, **McCarthy MI**, **McDowell IC**, **Mohammadi P**, **Monlong J**, **Montgomery SB**, **Muñoz-Aguirre M**, **Ndungu AW**, **Nicolae DL**, **Nobel AB**, **Oliva M**, **Ongen H**, **Palowitch JJ**, **Panousis N**, **Papasaikas P**, **Park Y**, **Parsana P**, **Payne AJ**, **Peterson CB**, **Quan J**, **Reverter F**, **Sabatti C**, **Saha A**, **Sammeth M**, **Scott AJ**, **Shabalin AA**, **Sodaei R**, **Stephens M**, **Stranger BE**, **Strober BJ**, **Sul JH**, **Tsang EK**, **Urbut S**, **Van De Bunt M**, **Wang G**, **Wen X**, **Wright FA**, **Xi HS**, **Yeger-Lotem E**, **Zappala Z**, **Zaugg JB**, **Zhou YH**, **Akey JM**, **Bates D**, **Chan J**, **Claussnitzer M**, **Demanelis K**, **Diegel M**, **Doherty JA**, **Feinberg AP**, **Fernando MS**, **Halow J**, **Hansen KD**, **Haugen E**, **Hickey PF**, **Hou L**, **Jasmine F**, **Jian R**, **Jiang L**, **Johnson A**, **Kaul R**, **Kellis M**, **Kibriya MG**, **Lee K**, **Li JB**, **Li Q**, **Lin J**, **Lin S**, **Linder S**, **Linke C**, **Liu Y**, **Maurano MT**, **Molinie B**, **Nelson J**, **Neri FJ**, **Park Y**, **Pierce BL**, **Rinaldi NJ**, **Rizzardi LF**, **Sandstrom R**, **Skol A**, **Smith KS**, **Snyder MP**, **Stamatoyannopoulos J**, **Tang H**, **Wang L**, **Wang M**, **Van Wittenberghe N**, **Wu F**, **Zhang R**, **Nierras CR**, **Branton PA**, **Carithers LJ**, **Guan P**, **Moore HM**, **Rao A**, **Vaught JB**, **Gould SE**, **Lockart NC**, **Martin C**, **Struewing JP**, **Volpi S**, **Addington AM**, **Koester SE**, **Little AR**, **Brigham LE**, **Hasz R**, **Hunter M**, **Johns C**, **Johnson M**, **Kopen G**, **Leinweber WF**, **Lonsdale JT**, **McDonald A**, **Mestichelli B**, **Myer K**, **Roe B**, **Salvatore M**, **Shad S**, **Thomas JA**, **Walters G**, **Washington M**, **Wheeler J**, **Bridge J**, **Foster BA**, **Gillard BM**, **Karasik E**, **Kumar R**, **Miklos M**, **Moser MT**, **Jewell SD**, **Montroy RG**, **Rohrer DC**, **Valley DR**, **Davis DA**, **Mash DC**, **Undale AH**, **Smith AM**, **Tabor DE**, **Roche N V.**, **McLean JA**, **Vatanian N**, **Robinson KL**, **Sobin L**, **Barcus ME**, **Valentino KM**, **Qi L**, **Hunter S**, **Hariharan P**, **Singh S**, **Um KS**, **Matose T**, **Tomaszewski MM**, **Barker LK**, **Mosavel M**, **Siminoff LA**, **Traino HM**, **Flicek P**, **Juettemann T**, **Ruffier M**, **Sheppard D**, **Taylor K**, **Trevanion SJ**, **Zerbino DR**, **Craft B**, **Goldman M**, **Haeussler M**, **Kent WJ**, **Lee CM**, **Paten B**, **Rosenbloom KR**, **Vivian J**, **Zhu J**, **Regev A**, **Ardlie KG**, **Hacohen N**, **MacArthur DG**. Landscape of X chromosome inactivation across human tissues. *Nature* 550: 244–248, 2017. doi: 10.1038/nature24265.

46. **Carrel L**, **Willard HF**. X-inactivation profile reveals extensive variability in X-linked gene expression in females. *Nature* 434: 400–404, 2005.

47. **Yang Z**, **Jiang X**, **Jiang X**, **Zhao H**. X-inactive-specific transcript: A long noncoding RNA with complex roles in human cancers. *Gene* 679: 28–35, 2018. doi: 10.1016/j.gene.2018.08.071.

48. **Wareham KA**, **Lyon MF**, **Glenister PH**, **Williams ED**. Age related reactivation of an X-linked gene. *Nature* 327: 725–727, 1987.

49. **Kostyunina DS**, **Rowan SC**, **Pakhomov N V.**, **Dillon E**, **Rochfort KD**, **Cummins PM**, **O'Rourke M**, **McLoughlin P**. Shear stress markedly alters the proteomic response to hypoxia in human pulmonary endothelial cells. *Am J Respir Cell Mol Biol* 68: 551–565,

2023.

50. **Bolger AM**, **Lohse M**, **Usadel B**. Trimmomatic: A flexible trimmer for Illumina sequence data. *Bioinformatics* 30: 2114–2120, 2014. doi: 10.1093/bioinformatics/btu170.

51. **Love MI**, **Huber W**, **Anders S**. Moderated estimation of fold change and dispersion for RNA-seq data with DESeq2. *Genome Biol* 15: 1–21, 2014. doi: 10.1186/s13059-014-0550-8.

52. **Cox J**, **Mann M**. MaxQuant enables high peptide identification rates, individualized p.p.b.-range mass accuracies and proteome-wide protein quantification. *Nat Biotechnol* 26: 1367–1372, 2008. doi: 10.1038/nbt.1511.

53. **Tyanova S**, **Temu T**, **Cox J**. The MaxQuant computational platform for mass spectrometry-based shotgun proteomics. *Nat Protoc* 11: 2301–2319, 2016. doi: 10.1038/nprot.2016.136.

54. **Cox J**, **Neuhauser N**, **Michalski A**, **Scheltema RA**, **Olsen J V.**, **Mann M**. Andromeda: A peptide search engine integrated into the MaxQuant environment. *J Proteome Res* 10: 1794–1805, 2011. doi: 10.1021/pr101065j.

55. **Tyanova S**, **Temu T**, **Sinitcyn P**, **Carlson A**, **Hein MY**, **Geiger T**, **Mann M**, **Cox J**. The Perseus computational platform for comprehensive analysis of (prote)omics data. *Nat Methods* 13: 731–740, 2016. doi: 10.1038/nmeth.3901.

56. **Tyanova S**, **Cox J**. Perseus: A Bioinformatics Platform for Integrative Analysis of Proteomics Data in Cancer Research. In: *von Stechow L. (eds) Cancer Systems Biology. Methods in Molecular Biology*. 2018, p. 133–148.

57. **Subramaniana A**, **Tamayoa P**, **Moothaa VK**, **Mukherjeed S**, **Eberta BL**, **Gillettea MA**, **Paulovichg A**, **Pomeroyh SL**, **Goluba TR**, **Landera ES**, **Mesirova JP**. Gene set enrichment analysis: A knowledge-based approach for interpreting genome-wide expression profiles. *PNAS* 102: 15545–15550, 2005. doi: 10.3969/j.issn.0372-2112.2018.08.016.

58. **Liberzon A**, **Birger C**, **Thorvaldsdóttir H**, **Ghandi M**, **Mesirov JP**, **Tamayo P**. The Molecular Signatures Database Hallmark Gene Set Collection. *Cell Syst* 1: 417–425, 2015. doi: 10.1016/j.cels.2015.12.004.

59. **Oliveros JC**. Venny. An interactive tool for comparing lists with Venn's diagrams. *https://bioinfogp.cnb.csic.es/tools/venny/index.html*: [date unknown].

60. **Guillon J**, **Petit C**, **Moreau M**, **Toutain B**, **Henry C**, **Roché H**, **Bonichon-Lamichhane N**, **Salmon JP**, **Lemonnier J**, **Campone M**, **Verrièle V**, **Lelièvre E**, **Guette C**, **Coqueret O**. Regulation of senescence escape by TSP1 and CD47 following chemotherapy treatment. *Cell Death Dis* 10, 2019. doi: 10.1038/s41419-019-1406-7.

61. **Arnaoutova I**, **Kleinman HK**. In vitro angiogenesis: Endothelial cell tube formation on gelled basement membrane extract. *Nat Protoc* 5: 628–635, 2010. doi: 10.1038/nprot.2010.6.

62. **Arnaoutova I**, **George J**, **Kleinman HK**, **Benton G**. The endothelial cell tube formation

assay on basement membrane turns 20: State of the science and the art. *Angiogenesis* 12: 267–274, 2009. doi: 10.1007/s10456-009-9146-4.

63. **Schneider CA**, **Rasband WS**, **Eliceiri KW**. NIH Image to ImageJ: 25 years of image analysis. *Nat Methods* 9: 671–675, 2012. doi: 10.1038/nmeth.2089.

64. **Ren B**, **Cam H**, **Takahashi Y**, **Volkert T**, **Terragni J**, **Young RA**, **Dynlacht BD**. E2F integrates cell cycle progression with DNA repair, replication, and G2/M checkpoints. *Genes Dev* 16: 245–256, 2002. doi: 10.1101/gad.949802.

65. **Vogel T**, **Cuo N**, **Krutzsch HC**, **Blake DA**, **Hartman J**, **Mendelovitz S**, **Panet A**, **Roberts DD**. Modulation of Endothelial Cell Proliferation , Adhesion , and Motility by Recombinant Heparin-Binding Domain and Synthetic Peptides From the Type Repeats of Thrombospondin. *J Cell Biochem* 53: 74–84, 1993.

66. **Penaloza D**, **Arias-Stella J**. The heart and pulmonary circulation at high altitudes: Healthy highlanders and chronic mountain sickness. *Circulation* 115: 1132–1146, 2007. doi: 10.1161/CIRCULATIONAHA.106.624544.

67. **Chaouat A**, **Naeije R**, **Weitzenblum E**. Pulmonary hypertension in COPD. *Eur Respir J* 32: 1371–1385, 2008. doi: 10.1183/09031936.00015608.

68. **Tielemans B**, **Delcroix M**, **Belge C**, **Quarck R**. TGFβ and BMPRII signalling pathways in the pathogenesis of pulmonary arterial hypertension. *Drug Discov Today* 24: 703–716, 2019. doi: 10.1016/j.drudis.2018.12.001.

69. **Pugliese SC**, **Poth JM**, **Fini MA**, **Olschewski A**, **El Kasmi KC**, **Stenmark KR**. The role of inflammation in hypoxic pulmonary hypertension: From cellular mechanisms to clinical phenotypes. *Am J Physiol - Lung Cell Mol Physiol* 308: L229–L252, 2015. doi: 10.1152/ajplung.00238.2014.

70. **Price LC**, **Wort SJ**, **Perros F**, **Dorfmüller P**, **Huertas A**, **Montani D**, **Cohen-Kaminsky S**, **Humbert M**. Inflammation in pulmonary arterial hypertension. *Chest* 141: 210–221, 2012. doi: 10.1378/chest.11-0793.

71. **Cullivan S**, **Murphy CA**, **Weiss L**, **Comer SP**, **Kevane B**, **Mccullagh B**, **Maguire PB**, **Fionnuala N**. Platelets , extracellular vesicles and coagulation in pulmonary arterial hypertension. *Pulm Circ* 11: 1–9, 2021. doi: 10.1177/20458940211021036.

72. **Good RB**, **Gilbane AJ**, **Trinder SL**, **Denton CP**, **Coghlan G**, **Abraham DJ**, **Holmes AM**. Endothelial to Mesenchymal Transition Contributes to Endothelial Dysfunction in Pulmonary Arterial Hypertension. *Am J Pathol* 185: 1850–1858, 2015. doi: 10.1016/j.ajpath.2015.03.019.

73. **Ventetuolo CE**, **Hess E**, **Austin ED**, **Barón AE**, **Klinger JR**, **Lahm T**, **Maddox TM**, **Plomondon ME**, **Thompson L**, **Zamanian RT**, **Choudhary G**, **Maron BA**. Sex-based differences in veterans with pulmonary hypertension: Results from the veterans affairs-clinical assessment reporting and tracking database. *PLoS One* 12: 1–15, 2017. doi: 10.1371/journal.pone.0187734.

74. **Carlsen J**, **Hasseriis Andersen K**, **Boesgaard S**, **Iversen M**, **Steinbrüchel D**, **Bøgelund Andersen C**. Pulmonary arterial lesions in explanted lungs after transplantation correlate with severity of pulmonary hypertension in chronic obstructive pulmonary

disease. *J Hear Lung Transplant* 32: 347–354, 2013. doi: 10.1016/j.healun.2012.11.014.

75. **Senger DR**, **Davis GE**. Angiogenesis. *Cold Spring Harb Perspect Biol* 3: 1–19, 2011.

76. **Howell K**, **Preston RJ**, **McLoughlin P**. Chronic hypoxia causes angiogenesis in addition to remodelling in the adult rat pulmonary circulation. *J Physiol* 547: 133–145, 2003. doi: 10.1113/jphysiol.2002.030676.

77. **Isenberg JS**, **Ridnour LA**, **Perruccio EM**, **Espey MG**, **Wink DA**, **Roberts DD**. Thrombospondin-1 inhibits endothelial cell responses to nitric oxide in a cGMP-dependent manner. *Proc Natl Acad Sci U S A* 102: 13141–13146, 2005. doi: 10.1073/pnas.0502977102.

78. **Isenberg JS**, **Wink DA**, **Roberts DD**. Thrombospondin-1 antagonizes nitric oxide-stimulated vascular smooth muscle cell responses. *Cardiovasc Res* 71: 785–793, 2006. doi: 10.1016/j.cardiores.2006.05.024.

79. **Isenberg JS**, **Romeo MJ**, **Yu C**, **Yu CK**, **Nghiem K**, **Monsale J**, **Rick ME**, **Wink DA**, **Frazier WA**, **Roberts DD**. Thrombospondin-1 stimulates platelet aggregation by blocking the antithrombotic activity of nitric oxide/cGMP signaling. *Blood* 111: 613–623, 2008. doi: 10.1182/blood-2007-06-098392.

80. **Rogers NM**, **Sharifi-Sanjani M**, **Yao M**, **Ghimire K**, **Bienes-Martinez R**, **Mutchler SM**, **Knupp HE**, **Baust J**, **Novelli EM**, **Ross M**, **Croix CS**, **Kutten JC**, **Czajka CA**, **Sembrat JC**, **Rojas M**, **Labrousse-Arias D**, **Bachman TN**, **Vanderpool RR**, **Zuckerbraun BS**, **Champion HC**, **Mora AL**, **Straub AC**, **Bilonick RA**, **Calzada MJ**, **Isenberg JS**. TSP1-CD47 signaling is upregulated in clinical pulmonary hypertension and contributes to pulmonary arterial vasculopathy and dysfunction. *Cardiovasc Res* 113: 15–29, 2017. doi: 10.1093/cvr/cvw218.

81. **Kaiser R**, **Frantz C**, **Bals R**, **Wilkens H**. The role of circulating thrombospondin-1 in patients with precapillary pulmonary hypertension. *Respir Res* 17: 4–13, 2016. doi: 10.1186/s12931-016-0412-x.

82. **Arnold AP**, **Breedlove SM**. Organizational and activational effects of sex steroids on brain and behavior: A reanalysis. *Horm Behav* 19: 469–498, 1985. doi: 10.1016/0018-506X(85)90042-X.

Figure Legends

Figure 1. Volcano plots showing differentially expressed genes (DEGs) and proteins (DEPs) between female and male HPMECs. **(A)** Volcano plot showing DEGs in female HPMECs compared to male HPMECs in normoxia (24 hours). **(B)** Volcano plot showing DEGs in female HPMECs compared to male HPMECs in hypoxia (24 hours). **(C)** Volcano plot showing DEGs in female HPMECs compared to male HPMECs in normoxia (48 hours). **(D)** Volcano plot showing DEGs in female HPMECs compared to male HPMECs in hypoxia (48 hours). DEGs (p adj<0.05, Wald test with Benjamini-Hochberg correction) that were expressed more highly in male HPMECs (n=3) are shown using blue symbols and have negative log_2fold-changes and those that are expressed more highly in female HPMECs (n=4) are shown using red symbols and have positive log_2fold-changes. The elipsoids (outlined by broken blue lines, A-D) encompass Y chromosome encoded DEGs. **(E)** Volcano plot showing DEPs in female HPMECs compared to male HPMECs in normoxia (24 hours). **(F)** Volcano plot showing DEPs in female HPMECs compared to male HPMECs in hypoxia (24 hours). **(G)** Volcano plot showing DEPs in female HPMECs compared to male HPMECs in normoxia (48 hours). **(H)** Volcano plot showing DEPs in female HPMECs compared to male HPMECs in hypoxia (48 hours). DEPs (p<0.05, T-test) that were expressed more highly in male HPMECs (n=3) are shown using pale blue symbols and have negative log_2fold-changes and those that were expressed more highly in female HPMECs (n=3) are shown using pale red symbols and have positive log_2fold-changes. Protein codes (Uniprot) were converted into gene names (Ensembl gene ID). Symbols with high absolute fold-change and/or low p value and those that represent potentially important targets were labelled with gene names.

Figure 2. Enriched pathways in male HPMECs (blue bars, n=3) and female HPMECs (red bars, n=3-4) in RNA sequencing and proteomics datasets. **(A)** Enriched pathways in normoxia (24 hours) in RNA sequencing dataset. **(B)** Enriched pathways in hypoxia (24 hours) in proteomics dataset. **(C)** Enriched pathways in normoxia (48 hours) in RNA sequencing dataset. **(D)** Enriched pathways in hypoxia (48 hours) in proteomics dataset. **(E)** Enriched pathways in normoxia (24 hours) in RNA sequencing dataset. **(F)** Enriched pathways in hypoxia (24 hours) in proteomics dataset. **(G)** Enriched pathways in normoxia (48 hours) in RNA sequencing dataset. **(H)** Enriched pathways in hypoxia (48 hours) in proteomics dataset. NES-normalised enrichment score, FDR-false discovery rate. FDR q value<0.05 was considered to be significant.

Figure 3. Pathways that were enriched (FDR q value<0.05) in female HPMECs (n=3-4) compared to male HPMECs (n=3) according to GSEA of the RNA sequencing and proteomics datasets after 24 and 48 hours of normoxia. The Epithelial-to-Mesenchymal Transition pathway was enriched in both RNA sequencing and proteomics data sets at both time points and the top ten leading edge genes and proteins (i.e. those that had the greatest influence on pathway enrichment) are shown in the associated box.

Figure 4. Pathways that were enriched (FDR q value<0.05) in female HPMECs (n=3-4) compared to male HPMECs (n=3) according to GSEA of the RNA sequencing and proteomics datasets after 24 and 48 hours of hypoxia. For the three pathways that were enriched in both RNA sequencing and proteomics datasets at the same time point(s), the top ten leading edge genes and proteins in those pathways (i.e. those that had the greatest influence on pathway enrichment) are shown in the associated boxes.

Figure 5. Pathways that were enriched (FDR q value<0.05) in male HPMECs (n=3) compared to female HPMECs (n=3-4) according to GSEA of the RNA sequencing and proteomics datasets after 24 and 48 hours of normoxia. For the two pathways that were enriched in both RNA sequencing and proteomics datasets at the same time point(s), the top ten leading edge genes and proteins in those pathways (i.e. those that had the greatest influence on pathway enrichment) are shown in the associated boxes.

Figure 6. (A-D) Proliferation rate assay on male (n=4) and female (n=5) HPMECs. **(A)** A representative image of the proliferation assay on male HPMECs in normoxia. **(B)** A representative image of the proliferation assay on female HPMECs in normoxia. Red – EdU-stained nuclei (synthesized during three hours of incubation with EdU after 24 hours of hypoxia or normoxia), green – Hoechst-stained nuclei (all nuclei). Images were taken using a 10x objective. **(C)** Percentage of new nuclei in normoxia. **(D)** Percentage of new nuclei in hypoxia. Data are presented as mean (SD). **(E-I)** Thrombospondin-1 mRNA and protein expression in male (n=5) and female (n=5) HPMECs. **(E)** Thrombospondin-1 (THBS1) mRNA expression in normoxia (24 hours), normalized to β-actin (ACTB) mRNA expression. **(F)** Thrombospondin-1 (THBS1) mRNA expression in hypoxia (24 hours), normalized to β-actin (ACTB) mRNA expression. **(G)** Thrombospondin-1 (THBS1) protein expression in normoxia (24 hours), normalized to β-actin (ACTB) protein expression. **(H)** Thrombospondin-1 (THBS1) protein expression in hypoxia (24 hours), normalized to β-actin (ACTB) protein expression. **(I)** A representative immunoblot image of thrombospondin-1 (THBS1) and β-actin proteins abundances for one donor of each sex is shown. Full membranes are presented in Appendix Figure 3. Data are presented as mean (SD). P values were calculated using t-test.

Appendix Figure 1. (A) Venn diagram showing RNAs and proteins that had higher expression in female HPMECs than in male HPMECs in RNA sequencing and proteomics datasets in normoxia. (B) Venn diagram showing RNAs and proteins that had lower expression in female HPMECs than in male HPMECs in RNA sequencing and proteomics datasets in normoxia. (C) Venn diagram showing RNAs and proteins that had higher expression in female HPMECs than in male HPMECs in RNA sequencing and proteomics datasets in hypoxia. (B) Venn diagram showing RNAs and proteins that had lower expression in female HPMECs than in male HPMECs in RNA sequencing and proteomics datasets in hypoxia.

Appendix Figure 2. Tube formation assay on male (n=4) and female (n=5) HPMECs. **(A)** A representative image of tube formation assay in male HPMECs in normoxia (one well) after five hours of tube formation assay. **(B)** A representative image of tube formation assay in female HPMECs in normoxia (one well) after five hours of tube formation assay. Images were taken using a 4x objective. **(C)** Average tube length in normoxia. **(D)** Average tube length in hypoxia. **(E)** Branching density in normoxia. **(F)** Branching density in hypoxia. Each symbol represents an average of five well replicates of an individual donor. Data are presented as mean (SD). P-values were calculated using t-test.

Appendix Figure 3. Full membranes of western blots of thrombospondin-1 (THBS1, 170 kDa) and β-actin (42 kDa). Lane 1 - Male 69 years old Normoxia, Lane 2- Female 56 years old Normoxia, Lane 3 - Male 69 years old Hypoxia, Lane 4 – Female 56 years old Hypoxia, Lane 5 – Male 62 years old Normoxia, Lane 6 – Female 64 years old Normoxia, Lane 7 – Male 62 years old Hypoxia, Lane 8 – Female 64 years old Hypoxia, Lane 9 – Male 60 years old Normoxia, Lane 10 Female 53 years old Normoxia, Lane 11 – Male 60 years old Hypoxia, Lane 12 – Female 53 years old Hypoxia, Lane 13 – Male 65 years old Normoxia, Lane 14 – Female 57 years old

853 Normoxia, Lane 15 – Male 65 years old Hypoxia, Lane 16 – Female 57 years old Hypoxia, Lane
854 17 – Male 56 years old Normoxia, Lane 18 – Female 70 years old Normoxia, Lane 19 – Male
855 56 years old Hypoxia, Lane 20 – Female 70 years old Hypoxia.

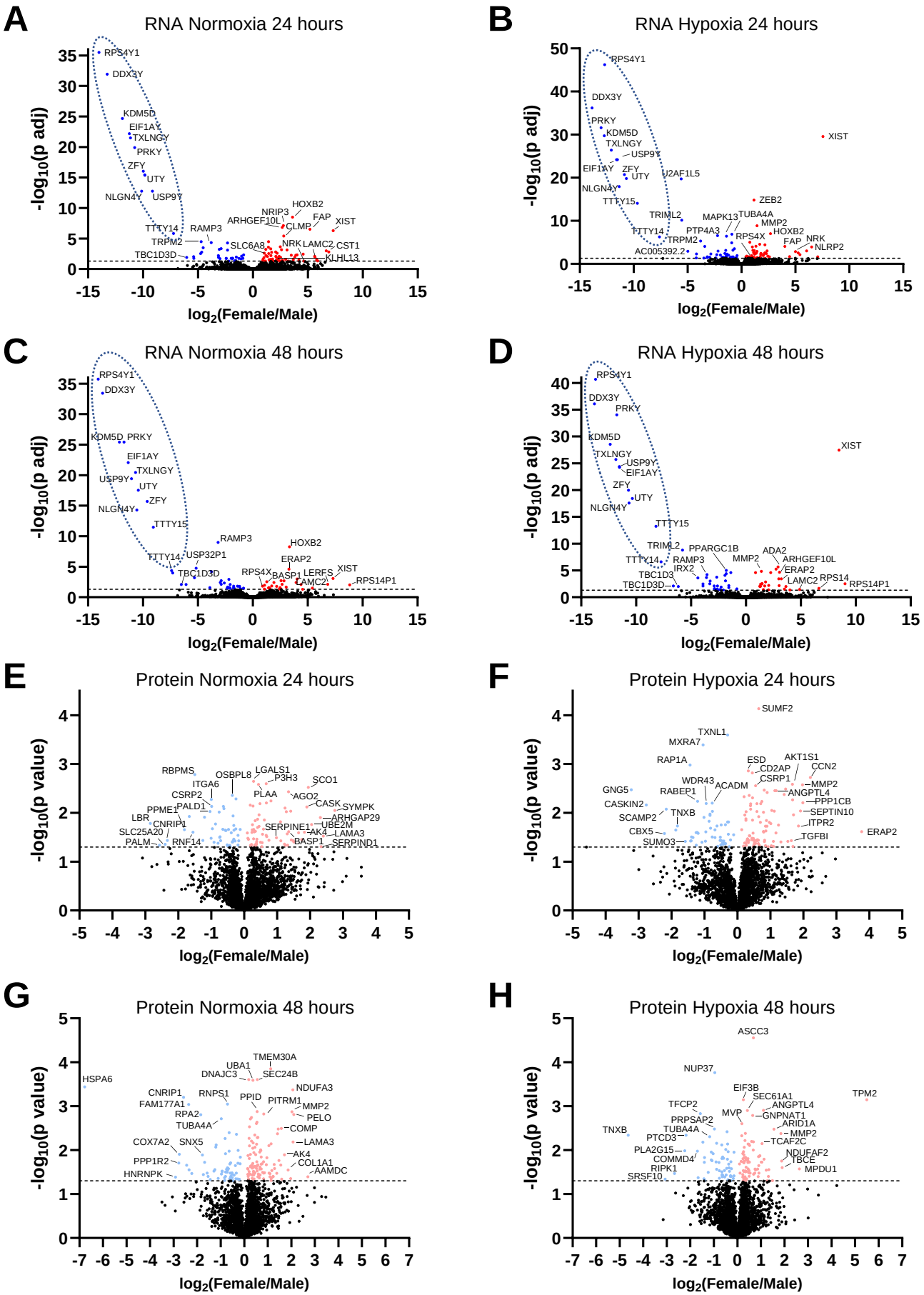

Figure 1

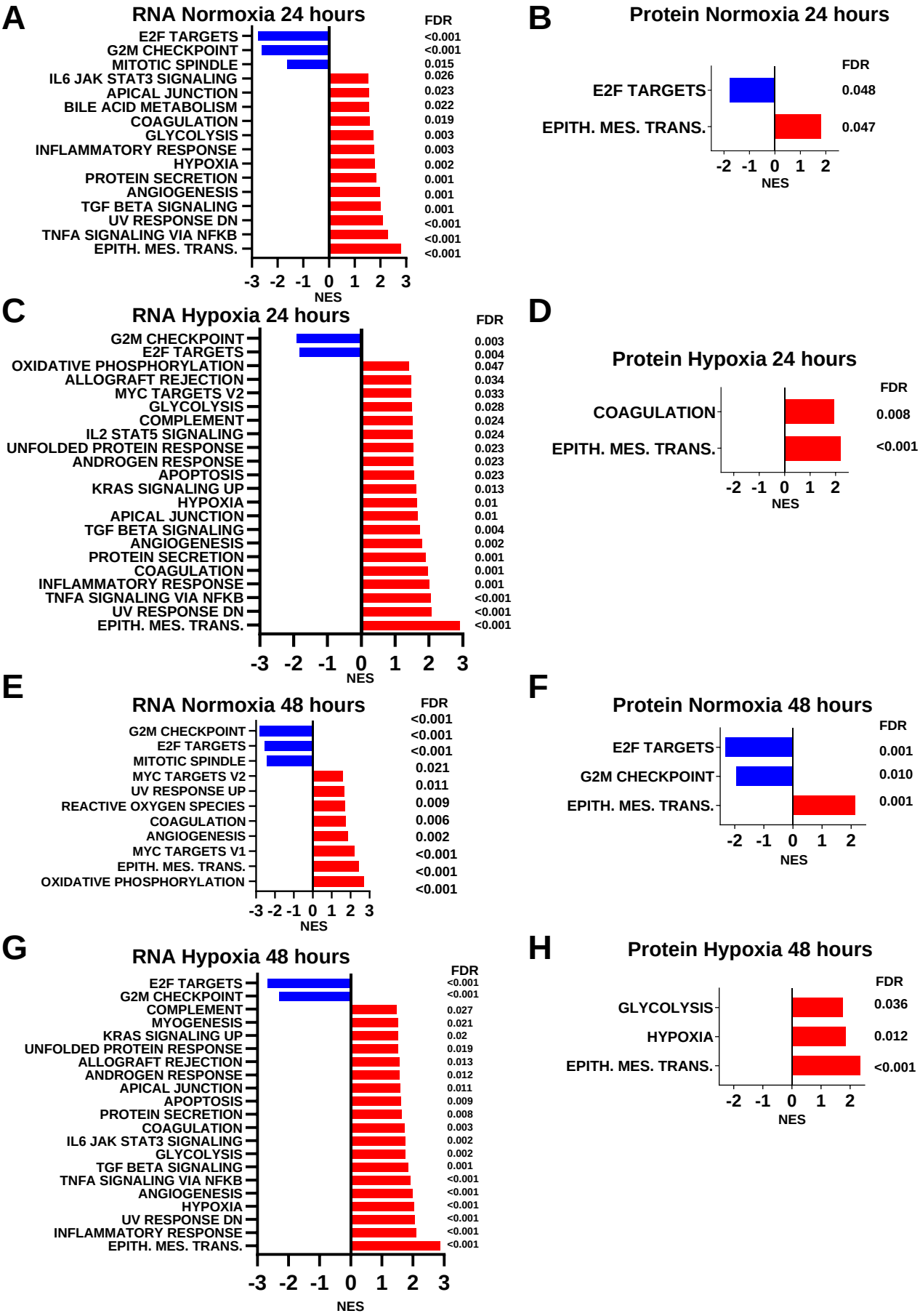

Figure 2

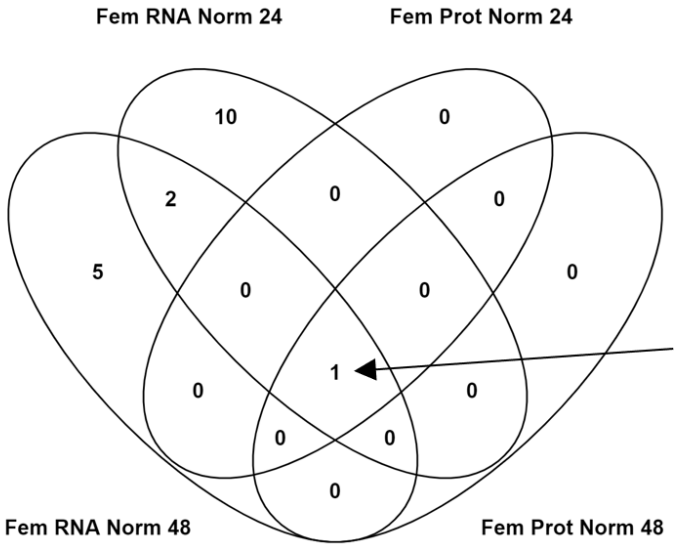

EPITHELIAL MESENCHYMAL TRANSITION:

RNA 24 h.: MMP2, LOXL1, SLC6A8, BASP1, PRRX1, LAMA2, CTHRC1, DPYSL3, BDNF, FGF2

Prot 24 h.: BASP1, THBS1, MMP2, SERPINE1, LAMA3, COL3A1, FSTL1, GJA1, TGFBI, ITGB3

RNA 48 h.: BASP1, LOXL1, MMP2, LAMA2, SLC6A8, MMP14, PRRX1, MSX1, CDH6, THBS1

Prot 48 h.: MMP2, LAMA3, BASP1, GJA1, SERPINE1, COL3A1, COMP, COL1A1, TGFBI, THBS1

Figure 3

EPITHELIAL MESENCHYMAL TRANSITION
RNA 24h.: MMP2, BASP1, DPYSL3, FGF2, PRRX1, COL12A1, MSX1, GEM, DKK1, GJA1
Prot 24h: CCN2, MMP2, THBS1, QSOX1, SERPINE1, COL5A1, TGFBI, CD44, POSTN, PLOD1
RNA 48 h.: MMP2, LOXL1, BASP1, LAMA2, PRRX1, CADM1, FSTL1, RHOB, SLC6A8, MSX1
Prot 48 h.: MMP2, TPM2, BASP1, SERPINE1, THBS1, PLOD1, PLOD2, COL5A1, CCN2, P3H1

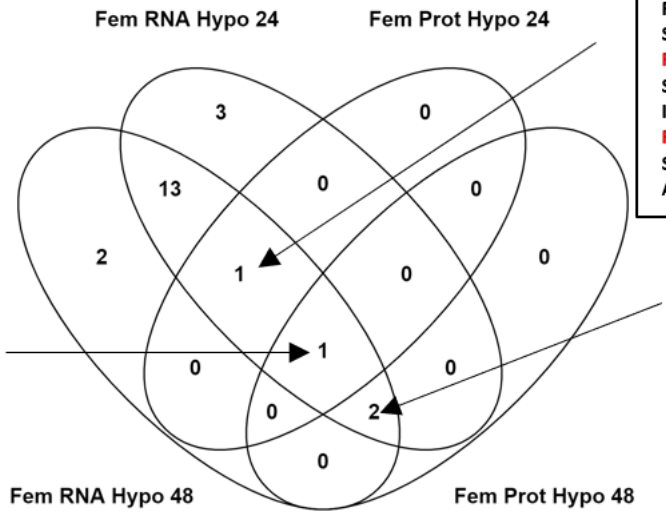

COAGULATION
RNA 24 h.: MMP2, PRSS23, CTSB, PLAU, CSRP1, MMP11, P2RY1, SERPINE1, FURIN, ARF4
RNA 48 h.: MMP2, MMP11, CTSB, SERPINE1, MMP14, PRSS23, CSRP1, ITGB3, CAPN5, PLAU
Prot 24 h.: MMP2, PRSS23, THBS1, SERPINE1, PLG, CSRP1, RAC1, CTSB, APOA1, C3

HYPOXIA
RNA 24 h.: EXT1, HOXB9, PFKFB3, SRPX, NDST2, GRHPR, COL5A1, TIPARP, HSPA5, IL6, CHST2
RNA 48 h.: CA12, SRPX, PFKFB3, P4HA2, SERPINE1, KIF5A, HK1, KDELR3, COL5A1, GYS1
Prot 48 h.: ANGPTL4, CAVIN3, SERPINE1, COL5A1, CCN2, HK2, MT2A, P4HA2, TGFBI, ERO1A

GLYCOLYSIS
RNA 24 h.: EXT1, FUT8, SRD5A3, HOMER1, PLOD1, COL5A1, HSPA5, CHST2, PDK3, PKP2
RNA 48 h. P4HA2, CACNA1H, SRD5A3, FUT8, IL13RA1, PLOD1, CAPN5, KDELR3, DSC2, COL5A1
Prot 48 h.: ANGPTL4, CYB5A, PLOD1, ALG1, PLOD2, COL5A1, HK2, P4HA2, TGFBI, ERO1A

Figure 4

E2F TARGETS

RNA 24 h. CDKN2C, ATAD2, TOP2A, PAN2, DSCC1, KIF18B, CDK1, SPAG5, ASF1B, SPC25

Prot 24 h.: DCTPP1, STMN1, LBR, RPA1, NASP, MCM3, HNRNPD, PCNA, SSRP1, CSE1L

RNA 48 h.: BARD1, HMMR, ATAD2, TOP2A, CDKN2C, DEPDC1, DLGAP5, CENPE, MKI67, BRCA2

Prot 48 h.: SMC4, RPA2, CDK1, CBX5, PHF5A, LBR, PRPS1, RPA1, SSRP1, HNRNPD

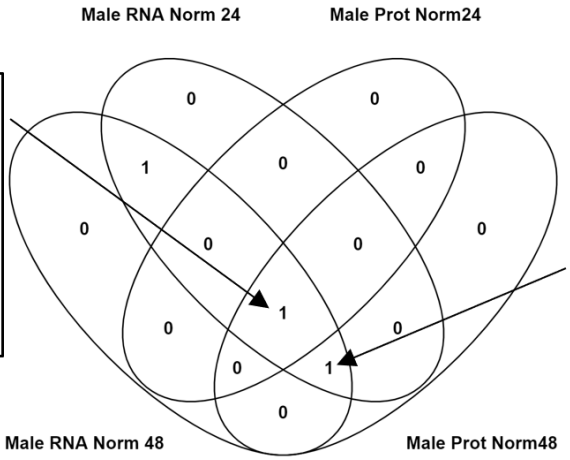

G2M CHECKPOINT

RNA 24h. CDKN2C, E2F2, TOP2A, NEK2, NDC80, KIF15, CDK1, TROAP, SMC2, RAD54L

RNA 48 h.: BARD1, HMMR, PRC1, KIF15, TOP2A, KIF11, CENPA, CDKN2C, KIF20B, CCNA2

Prot 48h.: SMC4, RPA2, CDK1, LBR, RBM14, HNRNPD, NASP, STMN1, LMNB1, H2AX

Figure 5

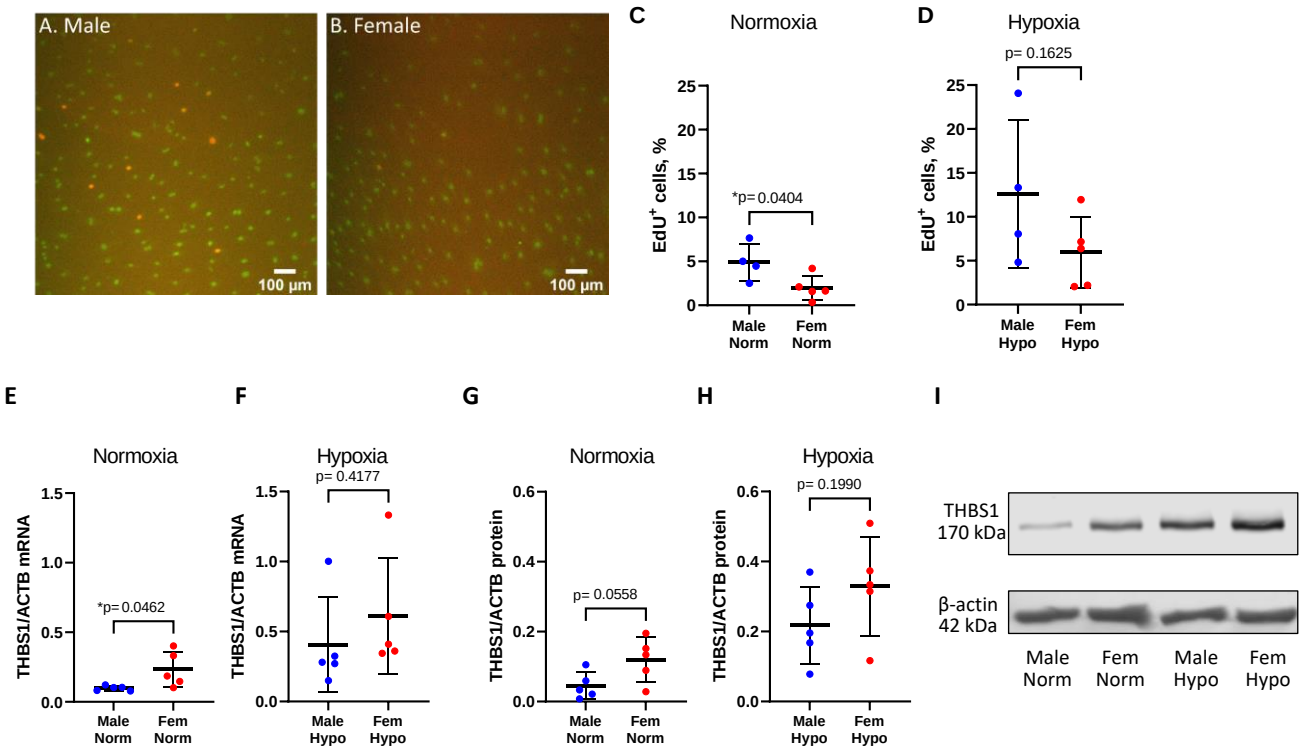

Figure 6

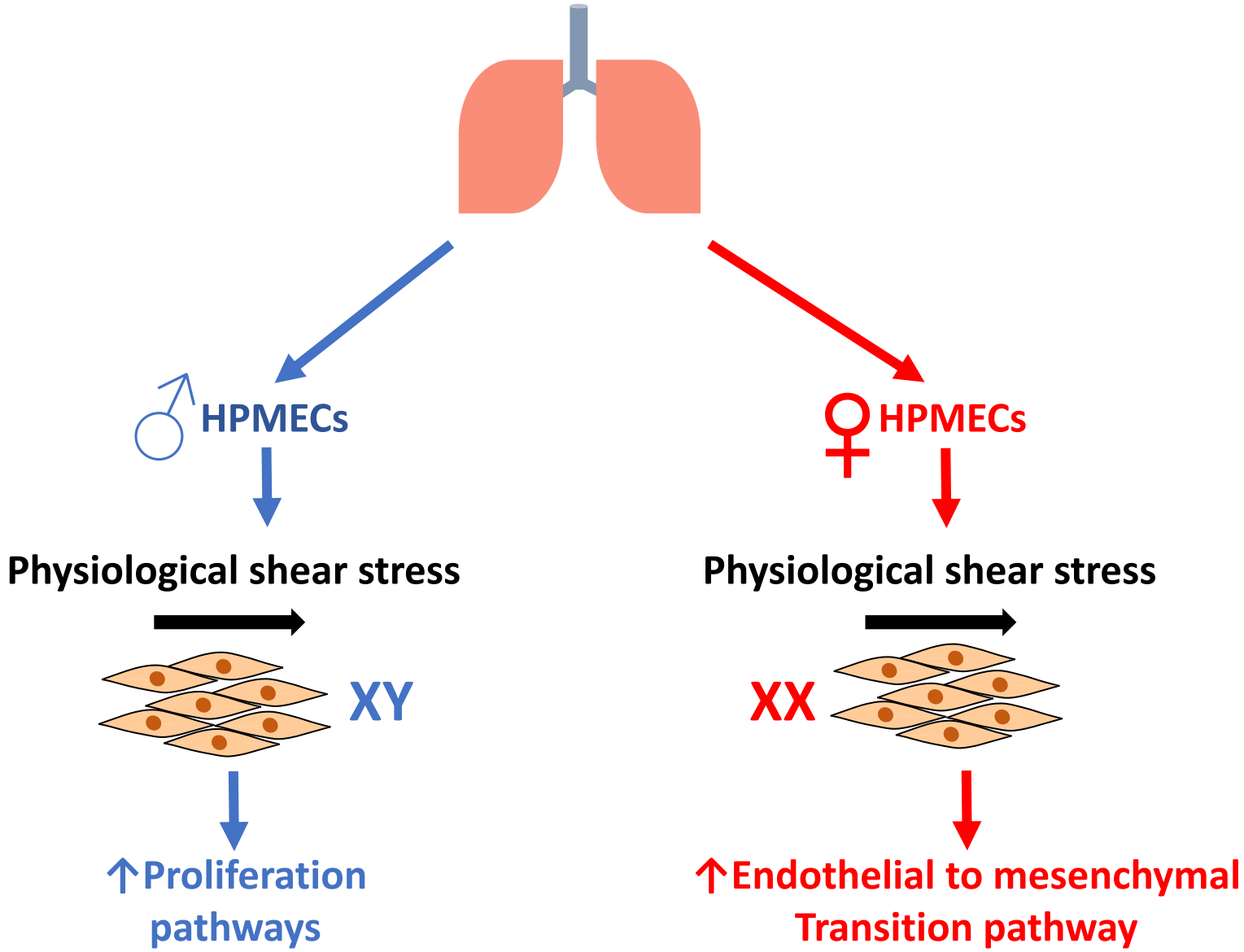

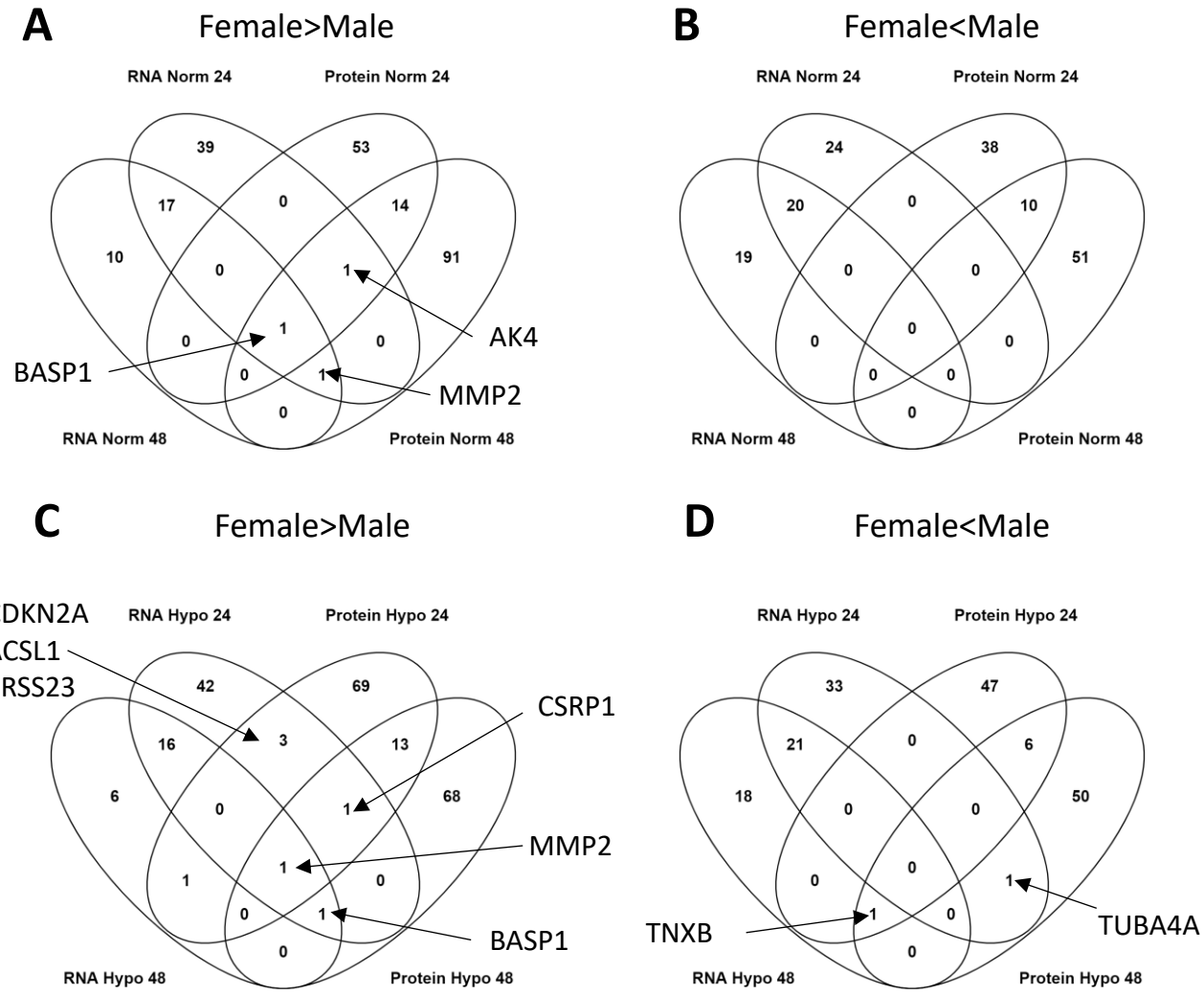

Appendix Figure 1

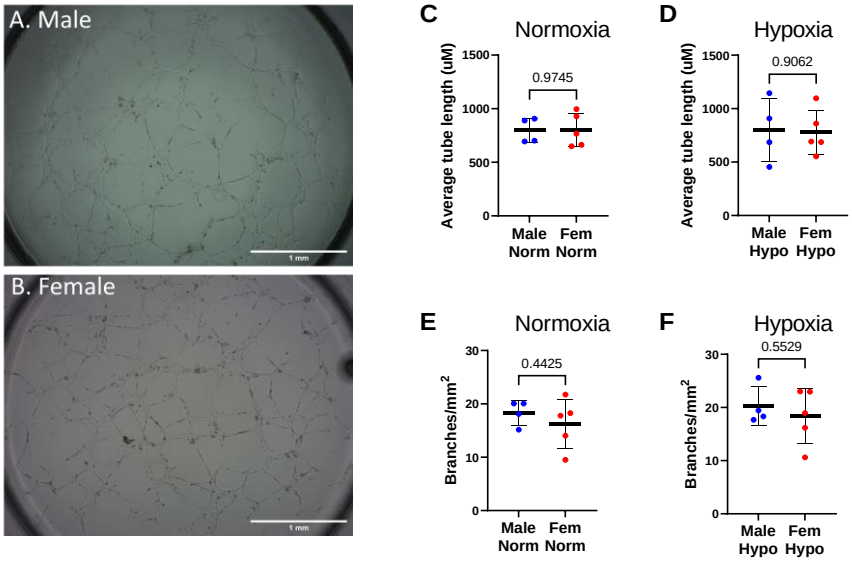

Appendix Figure 2

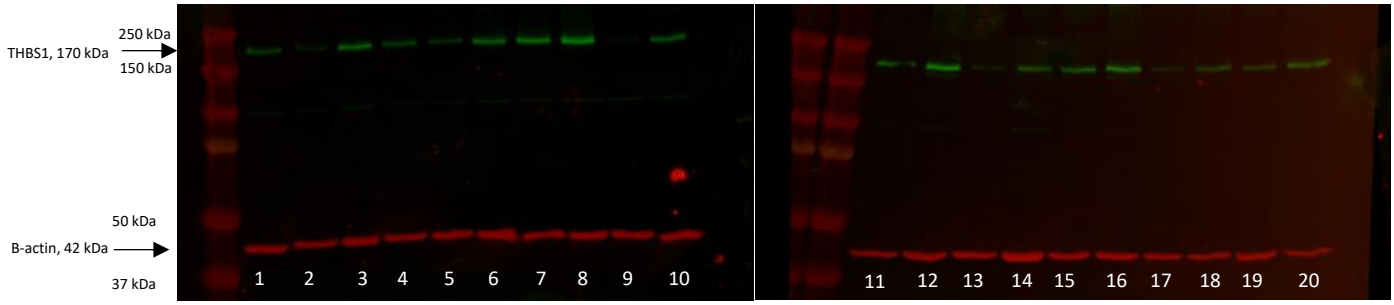

Appendix Figure 3

Appendix Table 1. Information about donors of HPMECs (Promocell, Germany) and the experiments in which each donor was used. All donors were non-smokers and Caucasians.

Sex	Age	Lot	Mass spec	RNA seq	Proliferation assay	Tube formation assay	RT-qPCR	Western Blot
Male	60	402Z030.1	✓	✓	✓	✓	✓	✓
Male	65	399Z027.2	✓	✓	✓	✓	✓	✓
Male	69	4073001.2	✓	✓	✓	✓	✓	✓
Male	62	466Z028.2			✓	✓	✓	✓
Male	56	474Z031.1					✓	✓
Female	53	438Z013.1	✓	✓	✓	✓	✓	✓
Female	56	4070302	✓	✓	✓	✓	✓	✓
Female	70	446Z002	✓	✓	✓	✓	✓	✓
Female	64	1071902.3		✓	✓	✓	✓	✓
Female	57	463Z013.1			✓	✓	✓	✓

Appendix Table 2. Differentially expressed genes in female HPMECs compared to male HPMECs in normoxia (24 hours).

Ensembl code	Gene	log2(Fem/Male)	p value	p adj
ENSG00000229807	XIST	7.308	4.49E-10	5.03E-07
ENSG00000170373	CST1	6.902	2.92E-06	0.001542
ENSG00000224114	RPS14P1	6.680	1.96E-06	0.001067
ENSG00000129514	FOXA1	5.896	0.000238	0.046585
ENSG00000170961	HAS2	5.803	0.000155	0.0335
ENSG00000121005	CRISPLD1	5.658	4.29E-05	0.012474
ENSG00000058085	LAMC2	5.626	2.34E-05	0.007966
ENSG00000078098	FAP	5.187	2.43E-10	2.91E-07
ENSG00000123572	NRK	4.641	0.000285	0.049764
ENSG00000128606	LRRC17	4.582	8.65E-06	0.003696
ENSG00000151617	EDNRA	4.185	0.000149	0.032587
ENSG00000165449	SLC16A9	4.030	1.18E-05	0.004854
ENSG00000116132	PRRX1	3.914	1.35E-05	0.005336
ENSG00000179242	CDH4	3.801	3.67E-05	0.011355
ENSG00000241186	TDGF1	3.668	0.000141	0.03118
ENSG00000173917	HOXB2	3.607	2.13E-12	3.18E-09
ENSG00000022556	NLRP2	3.497	1.37E-05	0.005336
ENSG00000080573	COL5A3	3.220	0.000264	0.048656
ENSG00000196876	SCN8A	3.106	1.23E-06	0.000714
ENSG00000164692	COL1A2	2.984	0.000108	0.025292
ENSG00000166250	CLMP	2.811	3.75E-09	3.74E-06
ENSG00000175352	NRIP3	2.767	5.52E-11	7.62E-08
ENSG00000109472	CPE	2.757	0.000246	0.046967
ENSG00000074964	ARHGEF10L	2.679	1.15E-10	1.48E-07
ENSG00000165029	ABCA1	2.675	0.000175	0.037349
ENSG00000175746	C15orf54	2.612	1.13E-06	0.000676
ENSG00000093072	ADA2	2.519	4.31E-05	0.012474
ENSG00000186235	LINC02610	2.485	2.88E-07	0.000225
ENSG00000111981	ULBP1	2.430	0.000263	0.048656
ENSG00000038945	MSR1	2.424	0.000228	0.045963
ENSG00000125657	TNFSF9	2.388	2.29E-05	0.007966
ENSG00000003096	KLHL13	2.308	7.04E-05	0.017918
ENSG00000105855	ITGB8	2.270	0.00011	0.025292
ENSG00000129038	LOXL1	2.213	5.37E-06	0.002537
ENSG00000100968	NFATC4	2.132	0.000195	0.040753
ENSG00000205213	LGR4	2.125	3.59E-05	0.011303
ENSG00000171016	PYGO1	2.100	2.35E-05	0.007966
ENSG00000159261	CLDN14	2.069	3.02E-06	0.001547
ENSG00000237238	BMS1P10	1.824	0.000269	0.048656
ENSG00000226476	LINC01748	1.791	0.0001	0.023932
ENSG00000230148	HOXB-AS1	1.783	0.000241	0.046585
ENSG00000135547	HEY2	1.709	3.64E-06	0.001763
ENSG00000060656	PTPRU	1.672	0.000286	0.049764

ENSG00000162433	AK4	1.640	1.7E-05	0.006343
ENSG00000152229	PSTPIP2	1.621	7.53E-07	0.0005
ENSG00000164932	CTHRC1	1.609	0.00012	0.027243
ENSG00000170775	GPR37	1.539	0.00024	0.046585
ENSG00000215126	CBWD6	1.483	0.000124	0.027806
ENSG00000185904	LINC00839	1.435	6.47E-06	0.002833
ENSG00000225138	SLC9A3-AS1	1.419	3.72E-08	3.33E-05
ENSG00000087245	MMP2	1.408	3.52E-07	0.000264
ENSG00000176788	BASP1	1.326	2.57E-05	0.008546
ENSG00000184588	PDE4B	1.199	1.73E-05	0.006349
ENSG00000169554	ZEB2	1.177	9.22E-07	0.000591
ENSG00000152760	DYNLT5	1.149	0.000268	0.048656
ENSG00000130821	SLC6A8	1.036	5.71E-06	0.002627
ENSG00000177663	IL17RA	1.007	4.73E-05	0.013459
ENSG00000162545	CAMK2N1	0.923	0.000109	0.025292
ENSG00000240356	RPL23AP7	0.902	0.0002	0.041277
ENSG00000125746	EML2	-0.845	1.19E-05	0.004854
ENSG00000176890	TYMS	-0.902	6.55E-05	0.017797
ENSG00000073605	GSDMB	-1.021	2.19E-05	0.007853
ENSG00000156802	ATAD2	-1.092	8.75E-05	0.021227
ENSG00000123080	CDKN2C	-1.273	6.95E-05	0.017918
ENSG00000131747	TOP2A	-1.502	3.32E-05	0.010638
ENSG00000186185	KIF18B	-1.556	0.000284	0.049764
ENSG00000163808	KIF15	-1.560	0.000235	0.046585
ENSG00000073350	LLGL2	-1.570	0.000218	0.044487
ENSG00000100376	FAM118A	-1.578	0.000194	0.040753
ENSG00000068078	FGFR3	-1.661	0.000271	0.048656
ENSG00000181804	SLC9A9	-1.845	7.09E-05	0.017918
ENSG00000205517	RGL3	-1.851	6.67E-05	0.01786
ENSG00000111087	GLI1	-1.980	6.19E-05	0.017344
ENSG00000253626	EIF5AL1	-2.196	0.000256	0.048335
ENSG00000167641	PPP1R14A	-2.301	1.45E-06	0.000811
ENSG00000067606	PRKCZ	-2.312	6.73E-08	5.49E-05
ENSG00000134323	MYCN	-2.427	6.79E-05	0.017918
ENSG00000114654	EFCC1	-2.429	7.31E-05	0.018215
ENSG00000156966	B3GNT7	-2.884	6.5E-07	0.000449
ENSG00000197859	ADAMTSL2	-2.990	8.3E-05	0.0204
ENSG00000118898	PPL	-3.061	9.7E-07	0.0006
ENSG00000142319	SLC6A3	-3.120	4.28E-05	0.012474
ENSG00000099994	SUSD2	-3.147	1.59E-05	0.006079
ENSG00000122679	RAMP3	-3.797	5.42E-08	4.63E-05
ENSG00000275895	U2AF1L5	-4.526	4.4E-07	0.000316
ENSG00000170561	IRX2	-4.653	3.32E-06	0.001652
ENSG00000142185	TRPM2	-4.714	3.63E-08	3.33E-05
ENSG00000231412	nan	-4.762	6.3E-06	0.002825
ENSG00000181541	MAB21L2	-5.376	6.32E-05	0.017459
ENSG00000179046	TRIML2	-5.396	2.83E-05	0.00924
ENSG00000274419	TBC1D3D	-6.033	4.1E-05	0.012457

ENSG00000176728	TTTY14	-7.222	1.41E-09	1.49E-06
ENSG00000233864	TTTY15	-9.142	1.06E-16	1.73E-13
ENSG00000114374	USP9Y	-9.826	2.07E-19	4.13E-16
ENSG00000183878	UTY	-9.845	1.66E-19	3.73E-16
ENSG00000067646	ZFY	-9.967	3.49E-20	8.95E-17
ENSG00000165246	NLGN4Y	-10.124	1.05E-16	1.73E-13
ENSG00000099725	PRKY	-10.756	4.29E-24	1.28E-20
ENSG00000131002	TXLNGY	-11.141	8.73E-26	3.13E-22
ENSG00000198692	EIF1AY	-11.247	1.43E-26	6.41E-23
ENSG00000012817	KDM5D	-11.872	3.64E-29	2.18E-25
ENSG00000067048	DDX3Y	-13.255	1.3E-36	1.16E-32
ENSG00000129824	RPS4Y1	-14.009	1.7E-40	3.05E-36

Appendix Table 3. Differentially expressed genes in female HPMECs compared to male HPMECs in hypoxia (24 hours).

Ensembl code	Gene	log2(Fem/Male)	p value	p adj
ENSG00000229807	XIST	7.560	8.73E-34	2.66E-30
ENSG00000198502	HLA-DRB5	7.068	0.000107	0.022023
ENSG00000022556	NLRP2	6.507	2.29E-07	0.000116
ENSG00000170373	CST1	6.042	2.42E-06	0.000971
ENSG00000058085	LAMC2	5.427	2.65E-05	0.006968
ENSG00000224114	AL591846.1	5.263	7.64E-06	0.00264
ENSG00000123572	NRK	5.004	3.79E-06	0.001373
ENSG00000165449	SLC16A9	4.463	9.94E-05	0.021039
ENSG00000078098	FAP	4.026	1.71E-07	9E-05
ENSG00000173917	HOXB2	2.699	1.04E-10	9.3E-08
ENSG00000093072	ADA2	2.588	0.000104	0.021722
ENSG00000196876	SCN8A	2.439	6.76E-05	0.015138
ENSG00000105855	ITGB8	2.381	2.34E-06	0.000964
ENSG00000074964	ARHGEF10L	2.311	1.36E-05	0.003914
ENSG00000166250	CLMP	2.219	8.87E-06	0.002874
ENSG00000163827	LRRC2	2.183	0.000383	0.049754
ENSG00000175352	NRIP3	2.168	6.5E-08	3.81E-05
ENSG00000186235	AC016757.1	2.152	8.02E-06	0.002656
ENSG00000225383	SFTA1P	2.061	2.71E-05	0.006989
ENSG00000159261	CLDN14	2.008	4.97E-05	0.011463
ENSG00000171016	PYGO1	1.813	1.19E-05	0.003638
ENSG00000205213	LGR4	1.812	1.35E-05	0.003914
ENSG00000170775	GPR37	1.793	2.79E-05	0.007082
ENSG00000228495	LINC01013	1.736	0.000117	0.023282
ENSG00000152229	PSTPIP2	1.684	4.44E-08	2.7E-05
ENSG00000118242	MREG	1.452	0.000202	0.032029
ENSG00000185904	LINC00839	1.443	3.33E-06	0.001239
ENSG00000087245	MMP2	1.438	1.42E-12	1.35E-09
ENSG00000147889	CDKN2A	1.403	0.000389	0.049754
ENSG00000145431	PDGFC	1.381	1.04E-05	0.003284
ENSG00000176788	BASP1	1.344	1.44E-07	8.1E-05
ENSG00000057019	DCBLD2	1.224	1.9E-05	0.005164
ENSG00000172458	IL17D	1.214	1.34E-05	0.003914
ENSG00000049130	KITLG	1.184	0.000228	0.034088
ENSG00000177663	IL17RA	1.184	1.78E-06	0.000754
ENSG00000145476	CYP4V2	1.178	7.8E-06	0.00264
ENSG00000169554	ZEB2	1.153	1.37E-18	1.61E-15
ENSG00000143797	MBOAT2	1.119	7.21E-06	0.002553
ENSG00000198246	SLC29A3	1.093	0.000141	0.025572
ENSG00000198598	MMP17	1.087	0.000162	0.028048
ENSG00000149177	PTPRJ	1.060	1.63E-06	0.000724
ENSG00000113657	DPYSL3	1.013	2.38E-07	0.000117
ENSG00000110218	PANX1	0.995	0.000192	0.030862

ENSG00000167703	SLC43A2	0.984	0.000231	0.034088
ENSG00000122778	KIAA1549	0.944	4.77E-05	0.011169
ENSG00000134986	NREP	0.933	0.000148	0.026242
ENSG00000107130	NCS1	0.897	0.000233	0.034088
ENSG00000138685	FGF2	0.877	0.000266	0.037705
ENSG00000100100	PIK3IP1	0.876	0.000258	0.037076
ENSG00000134874	DZIP1	0.874	0.000119	0.023282
ENSG00000087253	LPCAT2	0.777	1.43E-08	9.5E-06
ENSG00000151726	ACSL1	0.739	0.00022	0.033812
ENSG00000114554	PLXNA1	0.731	0.00017	0.028803
ENSG00000152137	HSPB8	0.723	0.000122	0.023492
ENSG00000150687	PRSS23	0.709	0.000128	0.024391
ENSG00000198034	RPS4X	0.669	0.000297	0.041523
ENSG00000082512	TRAF5	0.659	0.000191	0.030862
ENSG00000159176	CSRP1	0.659	0.000192	0.030862
ENSG00000141429	GALNT1	0.543	8.73E-05	0.018733
ENSG00000057252	SOAT1	0.489	0.000315	0.042867
ENSG00000144136	SLC20A1	0.469	7.26E-05	0.016035
ENSG00000157954	WIPI2	0.445	0.000183	0.030356
ENSG00000162618	ADGRL4	0.443	0.000141	0.025572
ENSG00000159593	NAE1	0.415	0.000135	0.025107
ENSG00000164284	GRPEL2	-0.413	5.22E-05	0.011878
ENSG00000130299	GTPBP3	-0.482	0.000267	0.037705
ENSG00000101040	ZMYND8	-0.649	0.000337	0.045046
ENSG00000078596	ITM2A	-0.666	6.4E-07	0.000304
ENSG00000271254	AC240274.1	-0.785	1.38E-06	0.000637
ENSG00000182310	SPACA6	-0.789	0.000119	0.023282
ENSG00000127824	TUBA4A	-0.888	1.52E-10	1.28E-07
ENSG00000215908	CROCCP2	-0.902	2.01E-08	1.28E-05
ENSG00000115657	ABCB6	-0.966	0.000144	0.025841
ENSG00000143603	KCNN3	-1.009	0.000315	0.042867
ENSG00000131634	TMEM204	-1.023	0.000231	0.034088
ENSG00000114378	HYAL1	-1.184	3.98E-05	0.009473
ENSG00000175691	ZNF77	-1.345	2.06E-05	0.005514
ENSG00000179855	GIPC3	-1.389	0.000132	0.024876
ENSG00000156711	MAPK13	-1.391	4.9E-10	3.73E-07
ENSG00000179403	VWA1	-1.395	3.37E-05	0.008274
ENSG00000124440	HIF3A	-1.432	8.73E-05	0.018733
ENSG00000155846	PPARGC1B	-1.455	0.000232	0.034088
ENSG00000120549	KIAA1217	-1.463	1.66E-06	0.000724
ENSG00000095637	SORBS1	-1.506	0.000388	0.049754
ENSG00000205464	ATP6AP1L	-1.525	0.000205	0.032262
ENSG00000144230	GPR17	-1.541	1.17E-05	0.003638
ENSG00000123358	NR4A1	-1.635	0.000216	0.033647
ENSG00000127311	HELB	-1.713	0.000176	0.029486
ENSG00000167641	PPP1R14A	-1.791	0.000164	0.028073
ENSG00000185168	LINC00482	-1.956	3.52E-05	0.008522
ENSG00000067606	PRKCZ	-2.167	2.65E-06	0.001035

ENSG00000184489	PTP4A3	-2.224	3.31E-10	2.65E-07
ENSG00000205517	RGL3	-2.286	2.99E-05	0.007454
ENSG00000272636	DOC2B	-2.380	0.000329	0.044308
ENSG00000111679	PTPN6	-2.429	0.00035	0.045954
ENSG00000197859	ADAMTSL2	-2.835	1.75E-05	0.004834
ENSG00000156966	B3GNT7	-2.961	0.000158	0.027729
ENSG00000104267	CA2	-3.178	0.000235	0.034088
ENSG00000099994	SUSD2	-3.182	0.000116	0.023282
ENSG00000122679	RAMP3	-3.404	1.71E-07	9E-05
ENSG00000115194	SLC30A3	-3.495	0.000341	0.045122
ENSG00000142185	TRPM2	-3.792	7.33E-09	5.07E-06
ENSG00000170561	IRX2	-4.169	1.69E-05	0.004759
ENSG00000183421	RIPK4	-4.189	0.000302	0.041756
ENSG00000231412	AC005392.2	-4.973	2.99E-06	0.001138
ENSG00000179046	TRIML2	-5.546	6.76E-14	6.87E-11
ENSG00000275895	U2AF1L5	-5.592	1.33E-23	1.84E-20
ENSG00000176728	TTTY14	-7.603	7.11E-10	5.16E-07
ENSG00000233864	TTTY15	-9.656	8.29E-18	9.02E-15
ENSG00000183878	UTY	-10.675	9.91E-24	1.51E-20
ENSG00000067646	ZFY	-10.857	1.08E-24	1.82E-21
ENSG00000165246	NLGN4Y	-11.334	8.68E-22	1.1E-18
ENSG00000198692	EIF1AY	-11.505	3.19E-28	6.6E-25
ENSG00000114374	USP9Y	-11.598	3.46E-28	6.6E-25
ENSG00000131002	TXLNGY	-12.072	1.63E-30	4.13E-27
ENSG00000129824	RPS4Y1	-12.699	3.94E-51	6.01E-47
ENSG00000012817	KDM5D	-12.730	5E-34	1.91E-30
ENSG00000099725	PRKY	-13.020	4.71E-36	2.39E-32
ENSG00000067048	DDX3Y	-13.855	8.3E-41	6.32E-37

Appendix Table 4. Differentially expressed genes in female HPMECs compared to male HPMECs in normoxia (48 hours).

Ensembl code	Gene	log2(Fem/Male)	p value	p adj
ENSG00000224114	RPS14P1	8.831	1.98E-05	0.009694
ENSG00000229807	XIST	7.302	8.82E-07	0.000818
ENSG00000234665	LERFS	6.831	1.39E-05	0.007834
ENSG00000058085	LAMC2	5.431	0.000101	0.032346
ENSG00000276600	RAB7B	4.544	0.000179	0.049664
ENSG00000179242	CDH4	4.384	1.56E-05	0.008034
ENSG00000165449	SLC16A9	4.047	1.2E-06	0.00106
ENSG00000078098	FAP	3.950	5.85E-06	0.003765
ENSG00000173917	HOXB2	3.338	3.74E-12	5.34E-09
ENSG00000164308	ERAP2	3.294	2.08E-08	2.57E-05
ENSG00000196876	SCN8A	3.046	5.47E-05	0.021456
ENSG00000074964	ARHGEF10L	2.844	2.81E-06	0.002086
ENSG00000093072	ADA2	2.669	1.3E-05	0.007567
ENSG00000175352	NRIP3	2.580	2.42E-06	0.001919
ENSG00000230148	HOXB-AS1	2.556	0.000182	0.049664
ENSG00000189058	APOD	2.538	0.00016	0.045565
ENSG00000159261	CLDN14	2.499	7.74E-05	0.02727
ENSG00000242265	PEG10	2.429	0.000153	0.044374
ENSG00000129038	LOXL1	2.177	3.82E-05	0.016121
ENSG00000100968	NFATC4	1.923	5.88E-06	0.003765
ENSG00000175746	C15orf54	1.720	3.1E-05	0.014367
ENSG00000170955	CAVIN3	1.544	0.000136	0.040667
ENSG00000185904	LINC00839	1.505	8.55E-05	0.028854
ENSG00000179862	CITED4	1.452	7.22E-05	0.02681
ENSG00000152229	PSTPIP2	1.448	8.97E-05	0.029723
ENSG00000176788	BASP1	1.278	4E-06	0.002856
ENSG00000154518	ATP5MC3	1.076	2.24E-05	0.010668
ENSG00000087245	MMP2	1.058	0.000169	0.04766
ENSG00000198034	RPS4X	0.887	3.61E-05	0.015842
ENSG00000164236	ANKRD33B	-0.838	0.000107	0.03323
ENSG00000184489	PTP4A3	-1.110	0.00014	0.041379
ENSG00000131747	TOP2A	-1.207	3.94E-05	0.016232
ENSG00000198901	PRC1	-1.222	4.38E-05	0.01767
ENSG00000072571	HMMR	-1.391	3.45E-05	0.015617
ENSG00000137460	FHDC1	-1.714	9.89E-05	0.032217
ENSG00000067606	PRKCZ	-1.739	3.67E-05	0.015842
ENSG00000148773	MKI67	-1.740	8.54E-05	0.028854
ENSG00000183856	IQGAP3	-2.052	0.000119	0.036275
ENSG00000205517	RGL3	-2.066	1.58E-05	0.008034
ENSG00000272636	DOC2B	-2.119	7.79E-05	0.02727
ENSG00000181804	SLC9A9	-2.169	1.38E-06	0.001166
ENSG00000114654	EFCC1	-2.202	7.6E-05	0.02727
ENSG00000205038	PKHD1L1	-2.294	5.55E-05	0.021456

ENSG00000186523	FAM86B1	-2.333	0.000107	0.03323
ENSG00000134323	MYCN	-2.599	7.66E-06	0.004742
ENSG00000244306	DUXAP10	-2.880	2.48E-06	0.001919
ENSG00000140022	STON2	-2.881	1.27E-05	0.007567
ENSG00000188385	JAKMIP3	-2.956	5.45E-06	0.003746
ENSG00000122679	RAMP3	-3.154	6.61E-13	1.02E-09
ENSG00000170160	CCDC144A	-3.764	5.8E-08	6.34E-05
ENSG00000215845	TSTD1	-3.914	7.07E-05	0.026779
ENSG00000188933	USP32P1	-5.155	1.31E-08	1.74E-05
ENSG00000179046	TRIML2	-5.300	6.74E-07	0.000658
ENSG00000186867	QRFPR	-6.077	1.52E-05	0.008034
ENSG00000274419	TBC1D3D	-6.502	1.6E-05	0.008034
ENSG00000266302	ENSG00000266302	-7.288	1.03E-07	0.000106
ENSG00000176728	TTTY14	-7.388	3.63E-08	4.21E-05
ENSG00000233864	TTTY15	-9.060	2.01E-15	3.4E-12
ENSG00000067646	ZFY	-9.608	9.53E-20	1.97E-16
ENSG00000183878	UTY	-10.428	1.25E-21	2.91E-18
ENSG00000165246	NLGN4Y	-10.550	2.7E-18	5.02E-15
ENSG00000131002	TXLNGY	-10.673	1.17E-24	3.62E-21
ENSG00000114374	USP9Y	-11.044	1.43E-23	3.79E-20
ENSG00000198692	EIF1AY	-11.341	2.28E-26	8.45E-23
ENSG00000012817	KDM5D	-11.724	7.67E-30	3.74E-26
ENSG00000099725	PRKY	-12.147	8.07E-30	3.74E-26
ENSG00000067048	DDX3Y	-13.683	3.99E-38	3.7E-34
ENSG00000129824	RPS4Y1	-14.069	9.81E-41	1.82E-36

Appendix Table 5. Differentially expressed genes in female HPMECs compared to male HPMECs in hypoxia (48 hours).

Ensembl code	Gene	log2(Fem/Male)	p value	p adj
ENSG00000224114	RPS14P1	9.025	5.64E-06	0.003098
ENSG00000229807	XIST	8.476	9.12E-32	3.61E-28
ENSG00000213058	nan	6.641	5.96E-05	0.02182
ENSG00000058085	LAMC2	4.886	0.000108	0.035691
ENSG00000165449	SLC16A9	4.010	0.000142	0.043313
ENSG00000078098	FAP	3.640	2.68E-05	0.010411
ENSG00000128602	SMO	3.507	8.77E-05	0.029926
ENSG00000164308	ERAP2	3.228	5.8E-07	0.000383
ENSG00000074964	ARHGEF10L	3.065	2.07E-08	2.15E-05
ENSG00000196876	SCN8A	3.033	1.38E-05	0.006518
ENSG00000180015	nan	2.991	5.7E-07	0.000383
ENSG00000093072	ADA2	2.920	1.73E-09	2.28E-06
ENSG00000173917	HOXB2	2.734	4.5E-09	5.57E-06
ENSG00000175352	NRIP3	2.266	2.85E-08	2.56E-05
ENSG00000074410	CA12	2.068	1.3E-05	0.006426
ENSG00000118242	MREG	2.055	0.000133	0.040977
ENSG00000129038	LOXL1	1.792	2.32E-06	0.00139
ENSG00000159261	CLDN14	1.702	1.73E-05	0.007798
ENSG00000145476	CYP4V2	1.589	0.000117	0.03788
ENSG00000152229	PSTPIP2	1.470	4.78E-06	0.00278
ENSG00000185904	LINC00839	1.454	6.07E-06	0.003245
ENSG00000087245	MMP2	1.414	1.32E-08	1.45E-05
ENSG00000177663	IL17RA	1.336	7.01E-06	0.003558
ENSG00000169554	ZEB2	1.320	2.36E-05	0.009533
ENSG00000176788	BASP1	1.266	2.36E-05	0.009533
ENSG00000146072	TNFRSF21	0.878	2.74E-08	2.56E-05
ENSG00000126790	L3HYPDH	-0.826	7.79E-05	0.027375
ENSG00000179855	GIPC3	-1.371	2.5E-08	2.47E-05
ENSG00000075213	SEMA3A	-1.558	1.38E-05	0.006518
ENSG00000073350	LLGL2	-1.560	4.3E-05	0.016039
ENSG00000100336	APOL4	-1.789	4.66E-08	4.01E-05
ENSG00000155846	PPARGC1B	-1.791	8.43E-09	9.81E-06
ENSG00000266714	MYO15B	-1.864	1.42E-06	0.000907
ENSG00000067606	PRKCZ	-1.903	1.07E-07	8.45E-05
ENSG00000272636	DOC2B	-2.058	0.000149	0.044701
ENSG00000125878	TCF15	-2.255	3.42E-05	0.013015
ENSG00000129450	SIGLEC9	-2.353	0.000119	0.03788
ENSG00000114654	EFCC1	-2.590	1.79E-05	0.007798
ENSG00000015413	DPEP1	-2.591	0.000125	0.03926
ENSG00000177363	LRRN4CL	-2.607	9.23E-05	0.030949
ENSG00000168477	TNXB	-2.665	2.39E-07	0.000182
ENSG00000156966	B3GNT7	-2.851	7.89E-05	0.027375
ENSG00000135077	HAVCR2	-2.861	6.99E-05	0.025163

ENSG00000183153	GJD3	-2.889	1.85E-05	0.007798
ENSG00000166856	GPR182	-3.257	1.54E-06	0.000949
ENSG00000275895	U2AF1L5	-3.299	5.37E-06	0.003035
ENSG00000122679	RAMP3	-3.537	7.42E-08	6.12E-05
ENSG00000134830	C5AR2	-3.595	2.96E-07	0.000217
ENSG00000231412	nan	-3.903	1.83E-05	0.007798
ENSG00000137726	FXYD6	-3.914	6.54E-06	0.003406
ENSG00000170561	IRX2	-4.376	3.53E-07	0.00025
ENSG00000179046	TRIML2	-5.782	1.02E-12	1.55E-09
ENSG00000274611	TBC1D3	-6.158	2.46E-05	0.009729
ENSG00000274419	TBC1D3D	-6.601	1.74E-05	0.007798
ENSG00000176728	TTTY14	-7.718	1.76E-10	2.49E-07
ENSG00000233864	TTTY15	-8.193	3.43E-17	5.66E-14
ENSG00000183878	UTY	-10.337	1.88E-22	3.72E-19
ENSG00000165246	NLGN4Y	-10.649	1.44E-21	2.58E-18
ENSG00000067646	ZFY	-10.691	5.02E-24	1.1E-20
ENSG00000198692	EIF1AY	-11.512	2.3E-28	5.68E-25
ENSG00000114374	USP9Y	-11.519	1.44E-28	4.07E-25
ENSG00000099725	PRKY	-11.752	1.32E-38	8.69E-35
ENSG00000131002	TXLNGY	-11.834	5.8E-30	1.91E-26
ENSG00000012817	KDM5D	-12.351	5.76E-33	2.85E-29
ENSG00000129824	RPS4Y1	-13.698	1.05E-45	2.08E-41
ENSG00000067048	DDX3Y	-13.795	7.79E-41	7.7E-37

Appendix Table 6. Differentially expressed proteins in female HPMECs compared to male HPMECs in normoxia (24 hours).

Uniprot code	Gene	Protein	log2(Fem/Male)	p value
Q92797	SYMPK	Symplekin	2.753	0.0089
A0A0A0MSA0	LAMA3	Laminin subunit alpha-3	2.401	0.0298
P05546	SERPIND1	Heparin cofactor 2	2.337	0.0495
Q52LW3	ARHGAP29	Rho GTPase-activating protein 29	2.315	0.0125
P61081	UBE2M	NEDD8-conjugating enzyme Ubc12	2.049	0.0174
J3QL56	SCO1	Protein SCO1 homolog, mitochondrial	1.945	0.0030
A0A2R8Y3B3	CASK	Peripheral plasma membrane protein CASK (Fragment)	1.904	0.0076
P27144	AK4	Adenylate kinase 4, mitochondrial	1.830	0.0248
E7ENN3	None	Nesprin-1	1.746	0.0352
B7Z2U2	TOM1L2	TOM1-like protein 2	1.654	0.0256
O14908	GIPC1	PDZ domain-containing protein GIPC1	1.508	0.0393
B3KPU0	PDLIM2	PDZ and LIM domain protein 2	1.486	0.0369
Q9UM00	TMCO1	Calcium load-activated calcium channel	1.433	0.0359
P19474	TRIM21	E3 ubiquitin-protein ligase TRIM21	1.416	0.0092
P80723	BASP1	Brain acid soluble protein 1	1.350	0.0242
Q9UKV8	AGO2	Protein argonaute-2	1.346	0.0037
P62633	CNBP	Cellular nucleic acid-binding protein	1.318	0.0461
A0A2R8YFH5	SEC23B	Protein transport protein SEC23	1.311	0.0270

A6NML8	None	Diaphanous homolog 2 (Drosophila), isoform CRA_c	1.283	0.0095
A0A3B3IRE4	DENND10	DENN domain-containing protein 10	1.255	0.0465
P07996	THBS1	Thrombospondin-1	1.244	0.0079
Q9UMX5	NENF	Neudesin	1.223	0.0437
P17050	NAGA	Alpha-N-acetylgalactosaminidase	1.112	0.0375
Q9Y2U8	LEMD3	Inner nuclear membrane protein Man1	1.103	0.0153
P05121	SERPINE1	Plasminogen activator inhibitor 1	0.982	0.0324
Q5JRX3	PITRM1	Presequence protease, mitochondrial	0.812	0.0057
Q9Y276	BCS1L	Mitochondrial chaperone BCS1	0.752	0.0363
P22033	MMUT	Methylmalonyl-CoA mutase, mitochondrial	0.689	0.0308
Q96EM0	L3HYPDH	Trans-3-hydroxy-L-proline dehydratase	0.676	0.0063
Q8IVL6	P3H3	Prolyl 3-hydroxylase 3	0.672	0.0025
Q9Y2D5	PALM2AKAP2	A-kinase anchor protein 2	0.669	0.0288
P63000	RAC1	Ras-related C3 botulinum toxin substrate 1	0.615	0.0139
Q86SF2	GALNT7	N-acetylgalactosaminyltransferase 7	0.588	0.0216
O15460	P4HA2	Prolyl 4-hydroxylase subunit alpha-2	0.557	0.0273
Q9Y3L5	RAP2C	Ras-related protein Rap-2c	0.550	0.0409
P16284	PECAM1	Platelet endothelial cell adhesion molecule	0.536	0.0492

P17812	CTPS1	CTP synthase 1	0.495	0.0399
A0A3B3ISH6	NOP9	Nucleolar protein 9 (Fragment)	0.482	0.0065
Q9BTM9	URM1	Ubiquitin-related modifier 1	0.455	0.0110
Q9UNP9	PPIE	Peptidyl-prolyl cis-trans isomerase E	0.451	0.0189
Q9Y263	PLAA	Phospholipase A-2-activating protein	0.437	0.0026
P22314	UBA1	Ubiquitin-like modifier-activating enzyme 1	0.408	0.0135
P21291	CSRP1	Cysteine and glycine-rich protein 1	0.408	0.0200
P62136	PPP1CA	Serine/threonine-protein phosphatase PP1-alpha catalytic subunit	0.385	0.0347
A0A087WVM4	MTHFD1L	Monofunctional C1-tetrahydrofolate synthase, mitochondrial	0.379	0.0387
P00338	LDHA	L-lactate dehydrogenase A chain	0.371	0.0421
Q9Y217	MTMR6	Myotubularin-related protein 6	0.370	0.0446
D3YTB1	RPL32	60S ribosomal protein L32 (Fragment)	0.351	0.0440
A0A087WTA5	None	Translation initiation factor eIF-2B subunit delta	0.350	0.0461
O95202	LETM1	Mitochondrial proton/calcium exchanger protein	0.345	0.0483
Q14257	RCN2	Reticulocalbin-2	0.339	0.0239
Q13347	EIF3I	Eukaryotic translation initiation factor 3 subunit I	0.335	0.0145
P30622	CLIP1	CAP-Gly domain-containing linker protein 1	0.326	0.0459

P00505	GOT2	Aspartate aminotransferase, mitochondrial	0.309	0.0245
O60664	PLIN3	Perilipin-3	0.307	0.0498
P60059	SEC61G	Protein transport protein Sec61 subunit gamma	0.290	0.0219
P09382	LGALS1	Galectin-1	0.287	0.0023
P62241	RPS8	40S ribosomal protein S8	0.286	0.0340
P20042	EIF2S2	Eukaryotic translation initiation factor 2 subunit 2	0.267	0.0073
A0A087WUT6	EIF5B	Eukaryotic translation initiation factor 5B	0.252	0.0175
O60313	OPA1	Dynamin-like 120 kDa protein, mitochondrial	0.248	0.0222
P13797	PLS3	Plastin-3	0.236	0.0252
Q15181	PPA1	Inorganic pyrophosphatase	0.226	0.0445
E5RJR5	SKP1	S-phase kinase-associated protein 1	0.219	0.0460
Q99460	PSMD1	26S proteasome non-ATPase regulatory subunit 1	0.192	0.0466
P63104	YWHAZ	14-3-3 protein zeta/delta	0.186	0.0069
O75822	EIF3J	Eukaryotic translation initiation factor 3 subunit J	0.132	0.0350
Q14690	PDCD11	Protein RRP5 homolog	0.116	0.0331
P53621	COPA	Coatomer subunit alpha	0.097	0.0259
Q8NE71	ABCF1	ATP-binding cassette sub-family F member 1	-0.117	0.0220
P61758	VBP1	Prefoldin subunit 3	-0.166	0.0375
O14980	XPO1	Exportin-1	-0.185	0.0458

O15511	ARPC5	Actin-related protein 2/3 complex subunit 5	-0.188	0.0288
Q15907	RAB11B	Ras-related protein Rab-11B	-0.247	0.0052
P30046	DDT	D-dopachrome decarboxylase	-0.251	0.0213
O75935	DCTN3	Dynactin subunit 3	-0.277	0.0376
P16435	POR	NADPH--cytochrome P450 reductase	-0.310	0.0227
Q5W0V3	FHIP2A	Protein FAM160B1	-0.313	0.0346
Q9Y2H0	DLGAP4	Disks large-associated protein 4	-0.315	0.0182
Q9H3S7	PTPN23	Tyrosine-protein phosphatase non-receptor type 23	-0.329	0.0372
Q13630	GFUS	GDP-L-fucose synthase	-0.335	0.0115
P07099	EPHX1	Epoxide hydrolase 1	-0.353	0.0398
Q9BZF1	OSBPL8	Oxysterol-binding protein-related protein 8	-0.359	0.0044
P17301	ITGA2	Integrin alpha-2	-0.359	0.0395
Q9UBQ0	VPS29	Vacuolar protein sorting-associated protein 29	-0.394	0.0256
Q02790	FKBP4	Peptidyl-prolyl cis-trans isomerase FKBP4	-0.418	0.0498
Q96JB5	CDK5RAP3	CDK5 regulatory subunit-associated protein 3	-0.435	0.0465
Q99615	DNAJC7	DnaJ homolog subfamily C member 7	-0.473	0.0219
Q9BWD1	ACAT2	Acetyl-CoA acetyltransferase, cytosolic	-0.501	0.0472
P55196	AFDN	Afadin	-0.512	0.0453
Q3KQV9	UAP1L1	UDP-N-acetylhexosamine pyrophosphorylase-like protein 1	-0.555	0.0231
O43491	EPB41L2	Band 4.1-like protein 2	-0.577	0.0226

O15230	LAMA5	Laminin subunit alpha-5	-0.616	0.0082
Q9BZL1	UBL5	Ubiquitin-like protein 5	-0.633	0.0074
A0A024RCR6	BAG6	BAG6	-0.645	0.0218
Q9NPD3	EXOSC4	Exosome complex component RRP41	-0.712	0.0371
P10301	RRAS	Ras-related protein R-Ras	-0.731	0.0308
Q15417	CNN3	Calponin-3	-0.740	0.0317
P68366	TUBA4A	Tubulin alpha-4A chain	-0.756	0.0096
O15247	CLIC2	Chloride intracellular channel protein 2	-0.794	0.0418
Q8TBF2	PRXL2B	Prostamide/prostaglandin F synthase	-0.871	0.0170
O00267	SUPT5H	Transcription elongation factor SPT5	-0.915	0.0402
A0A494C0G5	AGRN	Agrin	-0.964	0.0212
Q16527	CSRP2	Cysteine and glycine-rich protein 2	-0.984	0.0074
P23229	ITGA6	Integrin alpha-6	-0.999	0.0053
C9J6N5	FAM107B	Protein FAM107B (Fragment)	-1.002	0.0330
Q9ULE6	PALD1	Paladin	-1.037	0.0094
P55268	LAMB2	Laminin subunit beta-2	-1.204	0.0123
Q9Y5X3	SNX5	Sorting nexin-5	-1.251	0.0366
Q93062	RBPMS	RNA-binding protein with multiple splicing	-1.497	0.0016
Q9UBS8	RNF14	E3 ubiquitin-protein ligase RNF14	-1.553	0.0249
A0A2Q2TH77	None	Golgin subfamily A member 2	-1.662	0.0119
Q9Y570	PPME1	Protein phosphatase methylesterase 1	-1.815	0.0222
Q96F85	CNRIP1	CB1 cannabinoid receptor-interacting protein 1	-2.329	0.0369

O43772	SLC25A20	Mitochondrial carnitine/acylcarnitine carrier protein	-2.398	0.0443
O75781	PALM	Paralemmin-1	-2.570	0.0462
A0A494C1L1	LBR	Delta(14)-sterol reductase LBR	-2.847	0.0164

Appendix Table 7. Differentially expressed proteins in female HPMECs compared to male HPMECs in hypoxia (24 hours).

Uniprot code	Gene	Protein	log2(Fem/Male)	p value
Q6P179	ERAP2	Endoplasmic reticulum aminopeptidase 2	3.767	0.0243
P29279	CCN2	CCN family member 2	2.214	0.0019
P62140	PPP1CB	Serine/threonine-protein phosphatase PP1-beta catalytic subunit	1.985	0.0062
P08253	MMP2	72 kDa type IV collagenase	1.976	0.0027
E7EW69	SEPTIN10	Septin-10	1.914	0.0092
Q14571	ITPR2	Inositol 1,4,5-trisphosphate receptor type 2	1.850	0.0186
B7Z3Z9	ACSL1	Long-chain-fatty-acid--CoA ligase 1	1.705	0.0110
A0A3B3IS06	TCOF1	Treacle protein (Fragment)	1.684	0.0489
O15357	INPPL1	Phosphatidylinositol 3,4,5-trisphosphate 5-phosphatase 2	1.676	0.0054
Q96B36	AKT1S1	Proline-rich AKT1 substrate 1	1.670	0.0026
Q15582	TGFBI	Transforming growth factor-beta-induced protein ig-h3	1.636	0.0370
A0A0A0MR54	SCARF1	Scavenger receptor class F member 1	1.529	0.0384
O60331	PIP5K1C	Phosphatidylinositol 4-phosphate 5-kinase type-1 gamma	1.465	0.0032

O00391	QSOX1	Sulfhydryl oxidase 1	1.418	0.0042
J3QRG6	CDKN2A	Cyclin-dependent kinase inhibitor 2A	1.318	0.0394
G3V195	EML3	Echinoderm microtubule associated protein like 3, isoform CRA_c	1.245	0.0177
Q9BY76	ANGPTL4	Angiopoietin-related protein 4	1.174	0.0035
P82930	MRPS34	28S ribosomal protein S34, mitochondrial	1.168	0.0259
O95084	PRSS23	Serine protease 23	1.137	0.0035
Q9BV57	ADI1	1,2-dihydroxy-3-keto-5-methylthiopentene dioxygenase	1.121	0.0093
Q96QV1	HHIP	Hedgehog-interacting protein	1.095	0.0489
Q13363	CTBP1	C-terminal-binding protein 1	1.091	0.0383
F6PQP6	EPN2	Epsin-2 (Fragment)	1.041	0.0089
Q56VL3	OCIAD2	OCIA domain-containing protein 2	1.033	0.0472
P07996	THBS1	Thrombospondin-1	1.012	0.0166
P45985	MAP2K4	Dual specificity mitogen-activated protein kinase kinase 4	0.970	0.0157
O00469	PLOD2	Procollagen-lysine,2-oxoglutarate 5-dioxygenase 2	0.931	0.0495
P05121	SERPINE1	Plasminogen activator inhibitor 1	0.900	0.0038

Q9Y3L5	RAP2C	Ras-related protein Rap-2c	0.896	0.0188
P47914	RPL29	60S ribosomal protein L29	0.882	0.0144
D6RGE2	ISOC1	Isochorismatase domain-containing protein 1 (Fragment)	0.864	0.0235
Q9HD33	MRPL47	39S ribosomal protein L47, mitochondrial	0.853	0.0187
P30154	PPP2R1B	Serine/threonine-protein phosphatase 2A 65 kDa regulatory subunit A beta isoform	0.852	0.0469
P00747	PLG	Plasminogen	0.826	0.0364
B4DDF4	CNN2	Calponin	0.817	0.0387
Q6NUQ4	TMEM214	Transmembrane protein 214	0.811	0.0034
O75746	SLC25A12	Calcium-binding mitochondrial carrier protein Aralar1	0.796	0.0246
P04181	OAT	Ornithine aminotransferase, mitochondrial	0.794	0.0098
Q6PIU2	NCEH1	Neutral cholesterol ester hydrolase 1	0.792	0.0241
Q5NDL2	EOGT	EGF domain-specific O-linked N-acetylglucosamine transferase	0.743	0.0058
Q96KP1	EXOC2	Exocyst complex component 2	0.708	0.0065
Q8IVL6	P3H3	Prolyl 3-hydroxylase 3	0.700	0.0157
H0YD13	CD44	CD44 antigen	0.670	0.0464

Q8NBJ7	SUMF2	Inactive C-alpha-formylglycine-generating enzyme 2	0.650	0.0001
O95361	TRIM16	Tripartite motif-containing protein 16	0.647	0.0119
O60488	ACSL4	Long-chain-fatty-acid--CoA ligase 4	0.638	0.0366
Q14554	PDIA5	Protein disulfide-isomerase A5	0.636	0.0425
Q9UBQ7	GRHPR	Glyoxylate reductase/hydroxypyruvate reductase	0.611	0.0356
Q8NI22	MCFD2	Multiple coagulation factor deficiency protein 2	0.600	0.0371
I3L1L3	MYBBP1A	Myb-binding protein 1A (Fragment)	0.592	0.0094
Q86SF2	GALNT7	N-acetylgalactosaminyltransferase 7	0.590	0.0065
O95573	ACSL3	Long-chain-fatty-acid--CoA ligase 3	0.579	0.0364
P19623	SRM	Spermidine synthase	0.555	0.0423
P21291	CSRP1	Cysteine and glycine-rich protein 1	0.552	0.0028
Q9H993	ARMT1	Damage-control phosphatase ARMT1	0.518	0.0401
Q9BTU6	PI4K2A	Phosphatidylinositol 4-kinase type 2-alpha	0.511	0.0371
P00491	PNP	Purine nucleoside phosphorylase	0.508	0.0368
P55263	ADK	Adenosine kinase	0.501	0.0440

Q92542	NCSTN	Nicastrin	0.486	0.0336
B7ZC39	SH3GLB2	Endophilin-B2	0.480	0.0491
A2RRP1	NBAS	Neuroblastoma-amplified sequence	0.476	0.0260
P62136	PPP1CA	Serine/threonine-protein phosphatase PP1-alpha catalytic subunit	0.457	0.0049
P46778	RPL21	60S ribosomal protein L21	0.457	0.0141
Q9Y5K6	CD2AP	CD2-associated protein	0.455	0.0015
P08648	ITGA5	Integrin alpha-5	0.447	0.0354
Q6P2E9	EDC4	Enhancer of mRNA-decapping protein 4	0.441	0.0332
P17813	ENG	Endoglin	0.405	0.0084
O14617	AP3D1	AP-3 complex subunit delta-1	0.405	0.0065
Q8TAT6	NPLOC4	Nuclear protein localization protein 4 homolog	0.395	0.0071
B4DKY1	CARS1	Cysteinyl-tRNA synthetase 1	0.374	0.0296
O00303	EIF3F	Eukaryotic translation initiation factor 3 subunit F	0.361	0.0294
A0A590UJ56	CUL1	Cullin-1	0.360	0.0044
Q8N3C0	ASCC3	Activating signal cointegrator 1 complex subunit 3	0.352	0.0368

P30419	NMT1	Glycylpeptide N-tetradecanoyltransferase 1	0.333	0.0407
P10768	ESD	S-formylglutathione hydrolase	0.331	0.0014
P61086	UBE2K	Ubiquitin-conjugating enzyme E2 K	0.306	0.0340
Q9UN37	VPS4A	Vacuolar protein sorting-associated protein 4A	0.301	0.0347
Q8NFQ8	TOR1AIP2	Torsin-1A-interacting protein 2	0.294	0.0370
Q92616	GCN1	eIF-2-alpha kinase activator GCN1	0.272	0.0465
P18124	RPL7	60S ribosomal protein L7	0.264	0.0095
Q13488	TCIRG1	V-type proton ATPase 116 kDa subunit a isoform 3	0.261	0.0142
P00505	GOT2	Aspartate aminotransferase, mitochondrial	0.260	0.0133
P54136	RARS1	Arginine--tRNA ligase, cytoplasmic	0.258	0.0414
P36578	RPL4	60S ribosomal protein L4	0.224	0.0110
P28066	PSMA5	Proteasome subunit alpha type-5	0.222	0.0415
O95373	IPO7	Importin-7	0.200	0.0047
P17252	PRKCA	Protein kinase C alpha type	0.184	0.0482
O14976	GAK	Cyclin-G-associated kinase	0.133	0.0221
F8VY35	NAP1L1	Nucleosome assembly protein 1-like 1 (Fragment)	-0.112	0.0283

A0A0A0MRN5	OGFR	Opioid growth factor receptor	-0.211	0.0359
P01112	HRAS	GTPase HRas	-0.247	0.0494
P62820	RAB1A	Ras-related protein Rab-1A	-0.271	0.0154
P05023	ATP1A1	Sodium/potassium-transporting ATPase subunit alpha-1	-0.276	0.0275
O43396	TXNL1	Thioredoxin-like protein 1	-0.298	0.0003
P63151	PPP2R2A	Serine/threonine-protein phosphatase 2A 55 kDa regulatory subunit B alpha isoform	-0.299	0.0154
Q9BUL8	PDCD10	Programmed cell death protein 10	-0.360	0.0427
Q9H444	CHMP4B	Charged multivesicular body protein 4b	-0.362	0.0176
P20340	RAB6A	Ras-related protein Rab-6A	-0.378	0.0428
B0S8I6	FAM50A	Protein FAM50A (Fragment)	-0.385	0.0431
Q9NS69	TOMM22	Mitochondrial import receptor subunit TOM22 homolog	-0.413	0.0376
O75531	BANF1	Barrier-to-autointegration factor	-0.430	0.0417
P78536	ADAM17	Disintegrin and metalloproteinase domain-containing protein 17	-0.438	0.0442
P23634	ATP2B4	Plasma membrane calcium-transporting ATPase 4	-0.454	0.0414
Q86U42	PABPN1	Polyadenylate-binding protein 2	-0.491	0.0367

O60869	EDF1	Endothelial differentiation-related factor 1	-0.493	0.0177
E5RJR5	SKP1	S-phase kinase-associated protein 1	-0.505	0.0452
P62753	RPS6	40S ribosomal protein S6	-0.520	0.0314
Q6NVY1	HIBCH	3-hydroxyisobutyryl-CoA hydrolase, mitochondrial	-0.528	0.0367
P27105	STOM	Erythrocyte band 7 integral membrane protein	-0.598	0.0485
Q9Y5S9	RBM8A	RNA-binding protein 8A	-0.620	0.0186
Q9NP74	PALMD	Palmdelphin	-0.680	0.0222
P62328	TMSB4X	Thymosin beta-4	-0.683	0.0321
Q92930	RAB8B	Ras-related protein Rab-8B	-0.756	0.0093
B7Z9I1	None	Medium-chain-specific acyl-CoA dehydrogenase, mitochondrial	-0.764	0.0063
O95183	VAMP5	Vesicle-associated membrane protein 5	-0.767	0.0313
R9WNI0	FMR1	Fragile X mental retardation 1	-0.814	0.0207
Q9BVG4	PBDC1	Protein PBDC1	-0.830	0.0106
P23229	ITGA6	Integrin alpha-6	-0.831	0.0113
Q6ZRP7	QSOX2	Sulfhydryl oxidase 2	-0.856	0.0149
Q15061	WDR43	WD repeat-containing protein 43	-0.948	0.0064
Q08170	SRSF4	Serine/arginine-rich splicing factor 4	-0.957	0.0246

E9PD53	SMC4	Structural maintenance of chromosomes protein	-0.971	0.0382
Q8NFH4	NUP37	Nucleoporin Nup37	-1.012	0.0124
P84157	MXRA7	Matrix-remodeling-associated protein 7	-1.043	0.0004
E9PG46	AAK1	AP2-associated protein kinase 1	-1.073	0.0402
Q96EK5	KIFBP	KIF-binding protein	-1.194	0.0263
Q15276	RABEP1	Rab GTPase-binding effector protein 1	-1.208	0.0058
Q16831	UPP1	Uridine phosphorylase 1	-1.217	0.0253
P35052	GPC1	Glypican-1	-1.248	0.0459
G3V5X7	TEP1	Telomerase protein component 1	-1.253	0.0253
O14908	GIPC1	PDZ domain-containing protein GIPC1	-1.349	0.0321
O94804	STK10	Serine/threonine-protein kinase 10	-1.394	0.0311
E9PNM1	FDFT1	Squalene synthase	-1.405	0.0374
Q96HS1	PGAM5	Serine/threonine-protein phosphatase PGAM5, mitochondrial	-1.419	0.0377
P62834	RAP1A	Ras-related protein Rap-1A	-1.436	0.0010
P55854	SUMO3	Small ubiquitin-related modifier 3	-1.579	0.0385
A0A3B3ISX9	TNXB	Tenascin-X	-1.819	0.0186
Q9Y6A4	CFAP20	Cilia- and flagella-associated protein 20	-1.872	0.0225
O15127	SCAMP2	Secretory carrier-associated membrane protein 2	-2.157	0.0084
P45973	CBX5	Chromobox protein homolog 5	-2.215	0.0266
Q8WXE0	CASKIN2	Caskin-2	-2.764	0.0069

P63218	GNG5	Guanine nucleotide-binding protein G(I)/G(S)/G(O) subunit gamma-5	-3.218	0.0034

Appendix Table 8. Differentially expressed proteins in female HPMECs compared to male HPMECs in normoxia (48 hours).

Uniprot code	Gene	Protein	log2(Fem/Male)	p value
Q9H7C9	AAMDC	Mth938 domain-containing protein	2.702	0.0406
Q9BRX2	PELO	Protein pelota homolog	2.107	0.0016
A0A0A0MSA0	LAMA3	Laminin subunit alpha-3	2.069	0.0065
Q6FGG4	NDUFA3	NADH dehydrogenase (Ubiquinone) 1 alpha subcomplex, 3, 9kDa, isoform CRA_e	2.068	0.0004
P08253	MMP2	72 kDa type IV collagenase	2.029	0.0013
O43865	AHCYL1	S-adenosylhomocysteine hydrolase-like protein 1	1.969	0.0447
P02452	COL1A1	Collagen alpha-1(I) chain	1.860	0.0283
P27144	AK4	Adenylate kinase 4, mitochondrial	1.707	0.0128
Q15582	TGFBI	Transforming growth factor-beta-induced protein ig-h3	1.588	0.0456
G3XAP6	COMP	Cartilage oligomeric matrix protein	1.577	0.0032
Q9BY76	ANGPTL4	Angiopoietin-related protein 4	1.555	0.0219
A0A0G2JMS5	MRPL45	39S ribosomal protein L45, mitochondrial	1.476	0.0172
Q5T8A0	None	28S ribosomal protein S2, mitochondrial (Fragment)	1.443	0.0033

E7EU13	ARAP1	Arf-GAP with Rho-GAP domain, ANK repeat and PH domain-containing protein 1	1.411	0.0042
P07996	THBS1	Thrombospondin-1	1.379	0.0336
Q9NW15	ANO10	Anoctamin-10	1.287	0.0262
Q96GC9	VMP1	Vacuole membrane protein 1	1.269	0.0212
Q9C0C9	UBE2O	(E3-independent) E2 ubiquitin-conjugating enzyme	1.227	0.0406
P17302	GJA1	Gap junction alpha-1 protein	1.224	0.0395
O76071	CIAO1	Probable cytosolic iron-sulfur protein assembly protein CIAO1	1.172	0.0290
Q15714	TSC22D1	TSC22 domain family protein 1	1.144	0.0441
P25774	CTSS	Cathepsin S	1.142	0.0487
P82675	MRPS5	28S ribosomal protein S5, mitochondrial	1.141	0.0072
Q9NV96	TMEM30A	Cell cycle control protein 50A	1.121	0.0001
P05121	SERPINE1	Plasminogen activator inhibitor 1	1.094	0.0343
J3QRG6	CDKN2A	Cyclin-dependent kinase inhibitor 2A	1.091	0.0405
Q96BW9	TAMM41	Phosphatidate cytidylyltransferase, mitochondrial	1.052	0.0334

Q8IVL6	P3H3	Prolyl 3-hydroxylase 3	1.046	0.0079
P22681	CBL	E3 ubiquitin-protein ligase CBL	0.963	0.0150
Q96B36	AKT1S1	Proline-rich AKT1 substrate 1	0.940	0.0214
P80723	BASP1	Brain acid soluble protein 1	0.858	0.0328
Q14CX7	NAA25	N-alpha-acetyltransferase 25, NatB auxiliary subunit	0.832	0.0332
Q5JRX3	PITRM1	Presequence protease, mitochondrial	0.831	0.0015
H0YDT0	REPS1	RalBP1-associated Eps domain-containing protein 1 (Fragment)	0.821	0.0183
B7Z2U2	TOM1L2	TOM1-like protein 2	0.820	0.0449
O43660	PLRG1	Pleiotropic regulator 1	0.779	0.0320
O15460	P4HA2	Prolyl 4-hydroxylase subunit alpha-2	0.755	0.0204
Q8IWU5	SULF2	Extracellular sulfatase Sulf-2	0.723	0.0143
Q96BY6	DOCK10	Dedicator of cytokinesis protein 10	0.722	0.0266
Q96CS3	FAF2	FAS-associated factor 2	0.718	0.0208
Q6PIU2	NCEH1	Neutral cholesterol ester hydrolase 1	0.707	0.0102
Q9Y4E8	USP15	Ubiquitin carboxyl-terminal hydrolase 15	0.695	0.0099

A0A087WVM4	MTHFD1L	Monofunctional C1-tetrahydrofolate synthase, mitochondrial	0.670	0.0365
Q02809	PLOD1	Procollagen-lysine,2-oxoglutarate 5-dioxygenase 1	0.663	0.0242
Q9NX08	COMMD8	COMM domain-containing protein 8	0.657	0.0111
O95394	PGM3	Phosphoacetylglucosamine mutase	0.655	0.0271
O95302	FKBP9	Peptidyl-prolyl cis-trans isomerase FKBP9	0.643	0.0429
P16284	PECAM1	Platelet endothelial cell adhesion molecule	0.615	0.0379
Q9UBQ7	GRHPR	Glyoxylate reductase/hydroxypyruvate reductase	0.606	0.0349
P40222	TXLNA	Alpha-taxilin	0.581	0.0051
Q8WX93	PALLD	Palladin	0.578	0.0218
P16035	TIMP2	Metalloproteinase inhibitor 2	0.576	0.0404
O95487	SEC24B	Protein transport protein Sec24B	0.559	0.0002
Q86TU7	SETD3	Actin-histidine N-methyltransferase	0.559	0.0052
Q08752	PPID	Peptidyl-prolyl cis-trans isomerase D	0.546	0.0013
O00233	PSMD9	26S proteasome non-ATPase regulatory subunit 9	0.546	0.0298

Q16864	ATP6V1F	V-type proton ATPase subunit F	0.538	0.0023
Q15477	SKIV2L	Helicase SKI2W	0.537	0.0227
Q14257	RCN2	Reticulocalbin-2	0.531	0.0184
P51571	SSR4	Translocon-associated protein subunit delta	0.522	0.0073
Q96QV1	HHIP	Hedgehog-interacting protein	0.521	0.0025
B4DKY1	CARS1	Cysteinyl-tRNA synthetase 1	0.515	0.0260
Q9Y3D6	FIS1	Mitochondrial fission 1 protein	0.482	0.0126
O43847	NRDC	Nardilysin	0.458	0.0327
F5H365	SEC23A	Protein transport protein SEC23	0.457	0.0086
O95202	LETM1	Mitochondrial proton/calcium exchanger protein	0.448	0.0046
O75746	SLC25A12	Calcium-binding mitochondrial carrier protein Aralar1	0.447	0.0233
Q12792	TWF1	Twinfilin-1	0.421	0.0341
F8W717	EML1	Echinoderm microtubule-associated protein-like 1	0.416	0.0453
P61086	UBE2K	Ubiquitin-conjugating enzyme E2 K	0.413	0.0343
P21291	CSRP1	Cysteine and glycine-rich protein 1	0.410	0.0114
Q03001	DST	Dystonin	0.401	0.0246

Q15005	SPCS2	Signal peptidase complex subunit 2	0.397	0.0367
A0A0U1RQT1	ACAP2	Arf-GAP with coiled-coil, ANK repeat and PH domain-containing protein 2 (Fragment)	0.397	0.0463
O60884	DNAJA2	DnaJ homolog subfamily A member 2	0.390	0.0311
P08574	CYC1	Cytochrome c1, heme protein, mitochondrial	0.390	0.0304
O00764	PDXK	Pyridoxal kinase	0.381	0.0068
P52306	RAP1GDS1	Rap1 GTPase-GDP dissociation stimulator 1	0.375	0.0354
P30085	CMPK1	UMP-CMP kinase	0.370	0.0238
P22314	UBA1	Ubiquitin-like modifier-activating enzyme 1	0.369	0.0003
Q01970	PLCB3	1-phosphatidylinositol 4,5-bisphosphate phosphodiesterase beta-3	0.362	0.0091
P62854	RPS26	40S ribosomal protein S26	0.362	0.0201
Q9UQ35	SRRM2	Serine/arginine repetitive matrix protein 2	0.346	0.0373
Q15075	EEA1	Early endosome antigen 1	0.338	0.0258
Q969X5	ERGIC1	Endoplasmic reticulum-Golgi intermediate compartment protein 1	0.338	0.0216
Q9H8Y8	GORASP2	Golgi reassembly-stacking protein 2	0.337	0.0442
Q9C0C2	TNKS1BP1	182 kDa tankyrase-1-binding protein	0.311	0.0018

P21283	ATP6V1C1	V-type proton ATPase subunit C 1	0.308	0.0062
O43776	NARS1	Asparagine--tRNA ligase, cytoplasmic	0.303	0.0237
Q9UJW0	DCTN4	Dynactin subunit 4	0.275	0.0229
Q9NP61	ARFGAP3	ADP-ribosylation factor GTPase-activating protein 3	0.261	0.0020
O14579	COPE	Coatomer subunit epsilon	0.260	0.0238
P38646	HSPA9	Stress-70 protein, mitochondrial	0.260	0.0125
P41252	IARS1	Isoleucine--tRNA ligase, cytoplasmic	0.259	0.0354
Q9UMX0	UBQLN1	Ubiquilin-1	0.221	0.0080
Q99460	PSMD1	26S proteasome non-ATPase regulatory subunit 1	0.220	0.0029
P30050	RPL12	60S ribosomal protein L12	0.211	0.0155
Q32P28	P3H1	Prolyl 3-hydroxylase 1	0.207	0.0054
Q01813	PFKP	ATP-dependent 6-phosphofructokinase, platelet type	0.206	0.0354
P00558	PGK1	Phosphoglycerate kinase 1	0.204	0.0309
X6R9L0	DNAJC3	DnaJ homolog subfamily C member 3	0.192	0.0002
P53990	IST1	IST1 homolog	0.181	0.0452

Q09666	AHNAK	Neuroblast differentiation-associated protein AHNAK	0.171	0.0397
H3BPE1	MACF1	Microtubule-actin cross-linking factor 1, isoforms 1/2/3/5	0.163	0.0133
C9J9K3	RPSA	40S ribosomal protein SA (Fragment)	0.162	0.0495
P54578	USP14	Ubiquitin carboxyl-terminal hydrolase 14	0.158	0.0269
O14617	AP3D1	AP-3 complex subunit delta-1	0.154	0.0357
P43034	PAFAH1B1	Platelet-activating factor acetylhydrolase IB subunit alpha	0.147	0.0263
Q15366	PCBP2	Poly(rC)-binding protein 2	-0.164	0.0145
P50454	SERPINH1	Serpin H1	-0.173	0.0204
A0A087X020	None	Ribosome maturation protein SBDS	-0.203	0.0461
P30048	PRDX3	Thioredoxin-dependent peroxide reductase, mitochondrial	-0.260	0.0101
Q14974	KPNB1	Importin subunit beta-1	-0.268	0.0198
C9JNW5	RPL24	60S ribosomal protein L24	-0.278	0.0455
Q13185	CBX3	Chromobox protein homolog 3	-0.332	0.0043
I3L0H8	DDX19A	ATP-dependent RNA helicase DDX19A	-0.336	0.0334
E5RJR5	SKP1	S-phase kinase-associated protein 1	-0.351	0.0448
P62857	RPS28	40S ribosomal protein S28	-0.377	0.0224

P17301	ITGA2	Integrin alpha-2	-0.434	0.0372
Q6P9B6	MEAK7	MTOR-associated protein MEAK7	-0.482	0.0499
Q8WU76	SCFD2	Sec1 family domain-containing protein 2	-0.509	0.0424
P11498	PC	Pyruvate carboxylase, mitochondrial	-0.521	0.0330
P01112	HRAS	GTPase HRas	-0.525	0.0356
Q96PK6	RBM14	RNA-binding protein 14	-0.565	0.0411
P26006	ITGA3	Integrin alpha-3	-0.569	0.0396
E9PD53	SMC4	Structural maintenance of chromosomes protein	-0.579	0.0195
H3BPK3	HAGH	Hydroxyacylglutathione hydrolase, mitochondrial (Fragment)	-0.584	0.0486
P16435	POR	NADPH--cytochrome P450 reductase	-0.595	0.0334
O43491	EPB41L2	Band 4.1-like protein 2	-0.610	0.0206
Q4L180	FILIP1L	Filamin A-interacting protein 1-like	-0.612	0.0444
Q9BWD1	ACAT2	Acetyl-CoA acetyltransferase, cytosolic	-0.638	0.0040
P23229	ITGA6	Integrin alpha-6	-0.641	0.0105
Q9BT22	ALG1	Chitobiosyldiphosphodolichol beta-mannosyltransferase	-0.669	0.0265
O00442	RTCA	RNA 3-terminal phosphate cyclase	-0.711	0.0290
Q6UW02	CYP20A1	Cytochrome P450 20A1	-0.714	0.0252

H3BV80	RNPS1	RNA-binding protein with serine-rich domain 1	-0.715	0.0009
P63167	DYNLL1	Dynein light chain 1, cytoplasmic	-0.725	0.0318
A0A0B4J1Z1	SRSF7	Serine/arginine-rich-splicing factor 7	-0.749	0.0273
O43169	CYB5B	Cytochrome b5 type B	-0.791	0.0315
P10301	RRAS	Ras-related protein R-Ras	-0.797	0.0394
B4DRN8	ZDHHC20	Palmitoyltransferase	-0.799	0.0120
P17568	NDUFB7	NADH dehydrogenase [ubiquinone] 1 beta subcomplex subunit 7	-0.812	0.0054
Q8WYA6	CTNNBL1	Beta-catenin-like protein 1	-0.831	0.0487
Q9UJC5	SH3BGRL2	SH3 domain-binding glutamic acid-rich-like protein 2	-0.838	0.0425
F6U1T9	PPP3R1	Calcineurin subunit B type 1	-0.937	0.0309
Q9BY89	KIAA1671	Uncharacterized protein KIAA1671	-0.941	0.0301
A0A0C4DGN6	GIT1	ARF GTPase-activating protein GIT1	-0.966	0.0350
P68366	TUBA4A	Tubulin alpha-4A chain	-0.975	0.0019
Q9H553	ALG2	Alpha-1,3/1,6-mannosyltransferase ALG2	-1.107	0.0439
Q9UBW8	COPS7A	COP9 signalosome complex subunit 7a	-1.195	0.0076
P78318	IGBP1	Immunoglobulin-binding protein 1	-1.212	0.0085
Q13451	FKBP5	Peptidyl-prolyl cis-trans isomerase FKBP5	-1.246	0.0278
A0A286YFA2	PHGDH	D-3-phosphoglycerate dehydrogenase	-1.290	0.0301
Q9Y287	ITM2B	Integral membrane protein 2B	-1.446	0.0467
G3XAN4	TRAM1	Translocating chain-associated membrane protein 1	-1.535	0.0395

A0A024QZP7	CDK1	Cell division cycle 2, G1 to S and G2 to M, isoform CRA_a	-1.574	0.0335
Q9NZ45	CISD1	CDGSH iron-sulfur domain-containing protein 1	-1.686	0.0189
Q8WUY1	THEM6	Protein THEM6	-1.737	0.0361
Q9Y5X3	SNX5	Sorting nexin-5	-1.779	0.0129
P15927	RPA2	Replication protein A 32 kDa subunit	-1.850	0.0016
P14927	UQCRB	Cytochrome b-c1 complex subunit 7	-2.229	0.0340
A0A494C1L1	LBR	Delta(14)-sterol reductase LBR	-2.346	0.0280
G3V583	FAM177A1	Protein FAM177A1 (Fragment)	-2.360	0.0009
Q8WUF5	PPP1R13L	RelA-associated inhibitor	-2.447	0.0221
Q96F85	CNRIP1	CB1 cannabinoid receptor-interacting protein 1	-2.579	0.0006
P14406	COX7A2	Cytochrome c oxidase subunit 7A2, mitochondrial	-2.754	0.0125
E7EMN6	PPP1R2	Protein phosphatase inhibitor 2 (Fragment)	-2.778	0.0196
Q5T6W2	HNRNPK	Heterogeneous nuclear ribonucleoprotein K (Fragment)	-2.920	0.0411
P17066	HSPA6	Heat shock 70 kDa protein 6	-6.778	0.0004

Appendix Table 9. Differentially expressed proteins in female HPMECs compared to male HPMECs in hypoxia (48 hours).

Uniprot code	Gene	Protein	log2(Fem/Male)	p value
Q5TCU3	TPM2	Tropomyosin beta chain	5.496	0.0007
I3L405	MPDU1	Mannose-P-dolichol utilization defect 1 protein (Fragment)	2.634	0.0267
A0A2R8YHI9	TBCE	Tubulin-specific chaperone E	1.900	0.0249
Q8N183	NDUFAF2	NADH dehydrogenase [ubiquinone] 1 alpha subcomplex assembly factor 2	1.876	0.0177
P08253	MMP2	72 kDa type IV collagenase	1.850	0.0042
H0Y488	ARID1A	AT-rich interactive domain-containing protein 1A	1.550	0.0033
Q9BZ67	FRMD8	FERM domain-containing protein 8	1.491	0.0493
P07996	THBS1	Thrombospondin-1	1.330	0.0276
Q9P015	MRPL15	39S ribosomal protein L15, mitochondrial	1.315	0.0395
Q9C0C9	UBE2O	(E3-independent) E2 ubiquitin-conjugating enzyme	1.274	0.0499
Q969G5	CAVIN3	Caveolae-associated protein 3	1.223	0.0287
Q8IV08	PLD3	Phospholipase D3	1.129	0.0161

Q9BY76	ANGPTL4	Angiopoietin-related protein 4	1.110	0.0012
A0A1B0GVM2	TCAF2C	TRPM8 channel-associated factor 2C (Fragment)	1.049	0.0071
P49756	RBM25	RNA-binding protein 25	1.042	0.0187
P80723	BASP1	Brain acid soluble protein 1	1.018	0.0188
Q86SF2	GALNT7	N-acetylgalactosaminyltransferase 7	0.950	0.0135
P05121	SERPINE1	Plasminogen activator inhibitor 1	0.950	0.0134
O00469	PLOD2	Procollagen-lysine,2-oxoglutarate 5-dioxygenase 2	0.917	0.0334
Q5JTH9	RRP12	RRP12-like protein	0.902	0.0224
Q96QV1	HHIP	Hedgehog-interacting protein	0.895	0.0141
Q13322	GRB10	Growth factor receptor-bound protein 10	0.885	0.0401
Q8IUR0	TRAPPC5	Trafficking protein particle complex subunit 5	0.856	0.0271
Q02809	PLOD1	Procollagen-lysine,2-oxoglutarate 5-dioxygenase 1	0.772	0.0280
O15121	DEGS1	Sphingolipid delta(4)-desaturase DES1	0.750	0.0270
Q9UPN6	SCAF8	SR-related and CTD-associated factor 8	0.736	0.0332

Q13015	MLLT11	Protein AF1q	0.686	0.0353
P42765	ACAA2	3-ketoacyl-CoA thiolase, mitochondrial	0.682	0.0065
Q8N3C0	ASCC3	Activating signal cointegrator 1 complex subunit 3	0.679	0.0000
Q6PIU2	NCEH1	Neutral cholesterol ester hydrolase 1	0.676	0.0099
Q96EK6	GNPNAT1	Glucosamine 6-phosphate N-acetyltransferase	0.651	0.0016
C9JP16	CRTAP	Cartilage-associated protein	0.600	0.0063
H7C0E5	ZPR1	Zinc finger protein ZPR1 (Fragment)	0.544	0.0333
Q32P28	P3H1	Prolyl 3-hydroxylase 1	0.515	0.0078
Q6VY07	PACS1	Phosphofurin acidic cluster sorting protein 1	0.513	0.0188
B1AH87	TSPO	Putative peripheral benzodiazepine receptor-related protein (Fragment)	0.501	0.0391
Q9H993	ARMT1	Damage-control phosphatase ARMT1	0.494	0.0074
Q9P035	HACD3	Very-long-chain (3R)-3-hydroxyacyl-CoA dehydratase 3	0.492	0.0292
O95573	ACSL3	Long-chain-fatty-acid--CoA ligase 3	0.482	0.0329
Q96HE7	ERO1A	ERO1-like protein alpha	0.459	0.0267
Q9Y263	PLAA	Phospholipase A-2-activating protein	0.455	0.0073

O15258	RER1	Protein RER1	0.451	0.0191
P21291	CSRP1	Cysteine and glycine-rich protein 1	0.447	0.0157
Q96A65	EXOC4	Exocyst complex component 4	0.444	0.0175
P61619	SEC61A1	Protein transport protein Sec61 subunit alpha isoform 1	0.425	0.0013
P41250	GARS1	Glycine--tRNA ligase	0.393	0.0165
O15269	SPTLC1	Serine palmitoyltransferase 1	0.389	0.0451
Q03169	TNFAIP2	Tumor necrosis factor alpha-induced protein 2	0.386	0.0306
Q9H1I8	ASCC2	Activating signal cointegrator 1 complex subunit 2	0.370	0.0244
Q8TCU6	PREX1	Phosphatidylinositol 3,4,5-trisphosphate-dependent Rac exchanger 1 protein	0.369	0.0169
Q16537	PPP2R5E	Serine/threonine-protein phosphatase 2A 56 kDa regulatory subunit epsilon isoform	0.368	0.0487
P61019	RAB2A	Ras-related protein Rab-2A	0.364	0.0156
O75368	SH3BGRL	SH3 domain-binding glutamic acid-rich-like protein	0.349	0.0146
P22314	UBA1	Ubiquitin-like modifier-activating enzyme 1	0.347	0.0313
P41091	EIF2S3	Eukaryotic translation initiation factor 2 subunit 3	0.346	0.0494

Q86UU1	PHLDB1	Pleckstrin homology-like domain family B member 1	0.342	0.0297
Q8NFW8	CMAS	N-acylneuraminate cytidylyltransferase	0.341	0.0452
Q9NR12	PDLIM7	PDZ and LIM domain protein 7	0.337	0.0041
Q7KZF4	SND1	Staphylococcal nuclease domain-containing protein 1	0.325	0.0060
Q15008	PSMD6	26S proteasome non-ATPase regulatory subunit 6	0.319	0.0403
Q8NCW5	NAXE	NAD(P)H-hydrate epimerase	0.298	0.0149
J3KPX7	PHB2	Prohibitin	0.293	0.0086
Q8TAT6	NPLOC4	Nuclear protein localization protein 4 homolog	0.291	0.0184
Q9Y6M1	IGF2BP2	Insulin-like growth factor 2 mRNA-binding protein 2	0.285	0.0456
P62241	RPS8	40S ribosomal protein S8	0.283	0.0178
Q96AY3	FKBP10	Peptidyl-prolyl cis-trans isomerase FKBP10	0.280	0.0127
Q5T3Q7	HEATR1	HEAT repeat-containing protein 1	0.278	0.0150
P15880	RPS2	40S ribosomal protein S2	0.276	0.0195
P62136	PPP1CA	Serine/threonine-protein phosphatase PP1-alpha catalytic subunit	0.275	0.0306
Q96AC1	FERMT2	Fermitin family homolog 2	0.257	0.0108

P53618	COPB1	Coatomer subunit beta	0.255	0.0290
P15170	GSPT1	Eukaryotic peptide chain release factor GTP-binding subunit ERF3A	0.255	0.0187
P55884	EIF3B	Eukaryotic translation initiation factor 3 subunit B	0.255	0.0007
Q8TCJ2	STT3B	Dolichyl-diphosphooligosaccharide--protein glycosyltransferase subunit STT3B	0.248	0.0409
P41252	IARS1	Isoleucine--tRNA ligase, cytoplasmic	0.244	0.0497
Q01813	PFKP	ATP-dependent 6-phosphofructokinase, platelet type	0.236	0.0158
O75083	WDR1	WD repeat-containing protein 1	0.232	0.0119
Q9P2J5	LARS1	Leucine--tRNA ligase, cytoplasmic	0.231	0.0411
Q9H3P7	ACBD3	Golgi resident protein GCP60	0.226	0.0361
Q14764	MVP	Major vault protein	0.194	0.0025
Q5T4S7	UBR4	E3 ubiquitin-protein ligase UBR4	0.185	0.0047
P18124	RPL7	60S ribosomal protein L7	0.158	0.0181
P62714	PPP2CB	Serine/threonine-protein phosphatase 2A catalytic subunit beta isoform	0.116	0.0333
P50991	CCT4	T-complex protein 1 subunit delta	0.093	0.0206
O95425	SVIL	Supervillin	-0.145	0.0112

Q9UHD1	CHORDC1	Cysteine and histidine-rich domain-containing protein 1	-0.145	0.0384
O95865	DDAH2	N(G),N(G)-dimethylarginine dimethylaminohydrolase 2	-0.173	0.0443
Q9Y624	F11R	Junctional adhesion molecule A	-0.249	0.0264
P50502	ST13	Hsc70-interacting protein	-0.262	0.0395
F5GWT4	WNK1	Serine/threonine-protein kinase WNK1	-0.278	0.0183
P05023	ATP1A1	Sodium/potassium-transporting ATPase subunit alpha-1	-0.281	0.0494
O15230	LAMA5	Laminin subunit alpha-5	-0.291	0.0380
Q9NRV9	HEBP1	Heme-binding protein 1	-0.302	0.0398
Q15363	TMED2	Transmembrane emp24 domain-containing protein 2	-0.341	0.0304
P23588	EIF4B	Eukaryotic translation initiation factor 4B	-0.357	0.0252
A0A0A0MS51	GSN	Gelsolin	-0.366	0.0209
P33240	CSTF2	Cleavage stimulation factor subunit 2	-0.391	0.0108
P60468	SEC61B	Protein transport protein Sec61 subunit beta	-0.403	0.0472
Q9BWJ5	SF3B5	Splicing factor 3B subunit 5	-0.419	0.0072
A0A024R7W5	YTHDF3	YTH domain family, member 3, isoform CRA_a	-0.426	0.0160

Q32MZ4	LRRFIP1	Leucine-rich repeat flightless-interacting protein 1	-0.441	0.0038
O00592	PODXL	Podocalyxin	-0.456	0.0259
Q9UBI6	GNG12	Guanine nucleotide-binding protein G(I)/G(S)/G(O) subunit gamma-12	-0.480	0.0367
P14923	JUP	Junction plakoglobin	-0.492	0.0096
O14737	PDCD5	Programmed cell death protein 5	-0.544	0.0407
Q9NX58	LYAR	Cell growth-regulating nucleolar protein	-0.550	0.0292
P49593	PPM1F	Protein phosphatase 1F	-0.590	0.0153
Q9Y3L5	RAP2C	Ras-related protein Rap-2c	-0.624	0.0143
P84157	MXRA7	Matrix-remodeling-associated protein 7	-0.627	0.0374
Q9BRT3	MIEN1	Migration and invasion enhancer 1	-0.642	0.0403
Q96AP7	ESAM	Endothelial cell-selective adhesion molecule	-0.649	0.0359
Q9Y3U8	RPL36	60S ribosomal protein L36	-0.650	0.0380
Q96PY5	FMNL2	Formin-like protein 2	-0.654	0.0311
P10606	COX5B	Cytochrome c oxidase subunit 5B, mitochondrial	-0.657	0.0154
Q86VS8	HOOK3	Protein Hook homolog 3	-0.661	0.0076

Q5JVF3	PCID2	PCI domain-containing protein 2	-0.767	0.0295
Q16774	GUK1	Guanylate kinase	-0.769	0.0438
E9PPB5	C11orf54	Ester hydrolase C11orf54 (Fragment)	-0.779	0.0190
P27105	STOM	Erythrocyte band 7 integral membrane protein	-0.883	0.0272
R9WNI0	FMR1	Fragile X mental retardation 1	-0.885	0.0069
Q4L180	FILIP1L	Filamin A-interacting protein 1-like	-0.910	0.0186
Q8NFH4	NUP37	Nucleoporin Nup37	-0.963	0.0002
E7EPA1	PRPSAP2	Phosphoribosyl pyrophosphate synthase-associated protein 2 (Fragment)	-0.977	0.0033
A0A0C4DGH0	CD276	CD276 antigen	-1.031	0.0121
P35052	GPC1	Glypican-1	-1.077	0.0174
Q9BXP2	SLC12A9	Solute carrier family 12 member 9	-1.109	0.0166
O43169	CYB5B	Cytochrome b5 type B	-1.112	0.0111
P68366	TUBA4A	Tubulin alpha-4A chain	-1.181	0.0050
Q13573	SNW1	SNW domain-containing protein 1	-1.240	0.0321
Q13287	NMI	N-myc-interactor	-1.384	0.0488
O75431	MTX2	Metaxin-2	-1.396	0.0148
E9PN51	NDUFS8	NADH dehydrogenase [ubiquinone] iron-sulfur protein 8, mitochondrial (Fragment)	-1.403	0.0189

Q96AB6	NTAN1	Protein N-terminal asparagine amidohydrolase	-1.423	0.0451
Q9Y5Y7	LYVE1	Lymphatic vessel endothelial hyaluronic acid receptor 1	-1.468	0.0066
Q12800	TFCP2	Alpha-globin transcription factor CP2	-1.578	0.0015
Q16134	ETFDH	Electron transfer flavoprotein-ubiquinone oxidoreductase, mitochondrial	-1.666	0.0423
A0A0B4J287	COMMD4	COMM domain-containing protein 4	-1.702	0.0105
Q96EY7	PTCD3	Pentatricopeptide repeat domain-containing protein 3, mitochondrial	-2.183	0.0046
Q8NCC3	PLA2G15	Group XV phospholipase A2	-2.238	0.0103
Q13546	RIPK1	Receptor-interacting serine/threonine-protein kinase 1	-2.675	0.0341
Q5JRI1	SRSF10	Serine/arginine-rich-splicing factor 10	-3.067	0.0456
A0A3B3ISX9	TNXB	Tenascin-X	-4.640	0.0046